

40-A138 092

EXTRACTION OF ROTATION INFORMATION FROM A SIMULATED
FIBER OPTIC GYRO USI. (U) AIR FORCE INST OF TECH
WRIGHT-PATTERSON AFB OH SCHOOL OF ENGI. D J BRETT

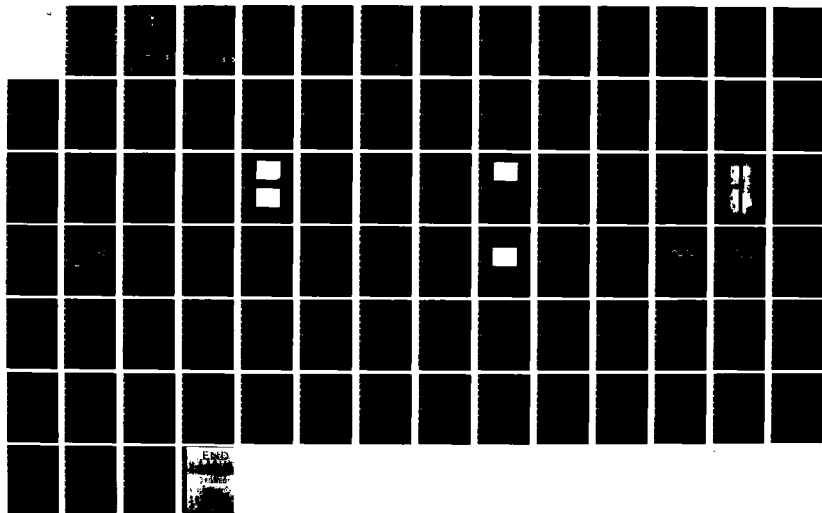
1/1

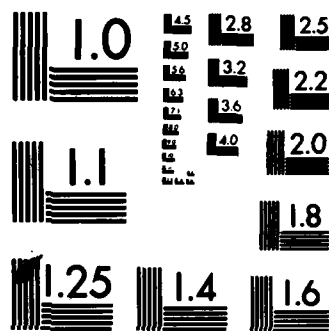
UNCLASSIFIED

DEC 83 AFIT/GE/EE/83D-12

F/G 1777

NL

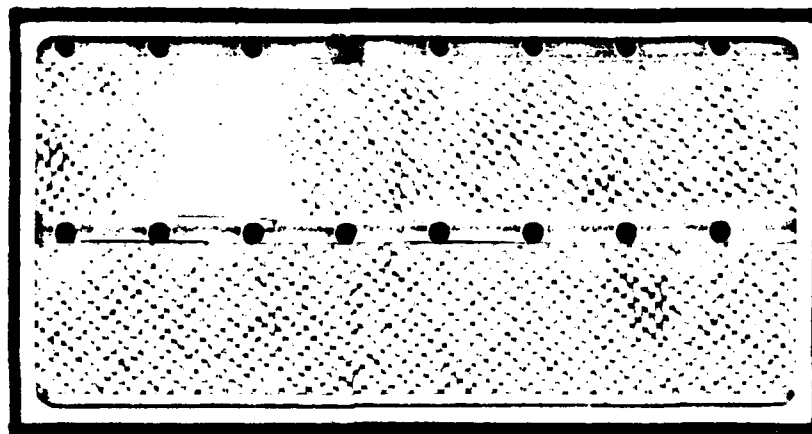




MICROCOPY RESOLUTION TEST CHART
NATIONAL BUREAU OF STANDARDS-1963-A

①

AD A138092



DISTRIBUTION STATEMENT A

Approved for public release;
Distribution Unlimited

DEPARTMENT OF THE AIR FORCE
AIR UNIVERSITY

AIR FORCE INSTITUTE OF TECHNOLOGY

Wright-Patterson Air Force Base, Ohio

DTIC
ELECTE
FEB 22 1984

S

B

DTIC FILE COPY

84 02 21 195

AFIT/GE/EE/83D-12

EXTRACTION OF ROTATION INFORMATION
FROM A SIMULATED FIBER OPTIC GYRO
USING AMPLITUDE MODULATION

THESIS

AFIT/GE/EE/83D-12

Daniel J. Brett
2Lt USAF

DTIC
ELECTE
S FEB 22 1984 D
B

Approved for public release; distribution unlimited

AFIT/GE/EE/83D-12

EXTRACTION OF ROTATION INFORMATION
FROM A SIMULATED FIBER OPTIC GYRO
USING AMPLITUDE MODULATION

THESIS

Presented to the Faculty of the School of Engineering
of the Air Force Institute of Technology

Air University

in Partial Fulfillment of the
Requirements for the Degree of
Master of Science

by

Daniel J. Brett, B.S.

2Lt

USAF

Graduate Electrical Engineering

December 1983

Approved for public release; distribution unlimited.

Contents

	<u>Page</u>
Preface	ii
List of Figures	iii
List of Tables	v
Abstract	vi
I. Introduction	1
Background	1
Problem and Scope	2
Assumptions	3
General Approach	4
Sequence of Presentation	5
II. Theory	6
Method of Amplitude Modulation	6
Significance of Data Obtained	11
General Layout of System	15
III. Experimental Setup	18
Introduction	18
Michelson Interferometer and Photodetector	18
S/H Circuit and A/D Converter	22
Digital Computer and D/A Converter	25
Summing and High Voltage Amplifiers	26
Summary	26
IV. Test Procedure	27
Introduction	27
Interferometer Alignment	27
Determination of Operating Points	28
Hardware Limits	30
Software Development	30
Data Collecting	34
V. Results	40
VI. Conclusions and Recommendations	47
Bibliography	49
Appendix A: Sagnac Effect	50
Appendix B: Sagnac Interferometer	53

Contents

(Continued)

	<u>Page</u>
Appendix C: Hardware Descriptions	60
Appendix D: Control Program Coding	64
Vita	73



Accession For	
NTIS GRA&I	<input checked="checked" type="checkbox"/>
DTIC TAB	<input type="checkbox"/>
Unannounced	<input type="checkbox"/>
Justification	
By	
Distribution/	
Availability Codes	
Dist	Avail and/or Special
A-1	

Preface

This study was conducted to determine the feasibility of a new concept for extracting rotation information from a fiber optic gyro. This method is attractive because it also provides laser wavelength change information as well as detection of changes in laser intensity.

Several weeks into the project, it became evident that building a fiber optic gyro would consume all the time needed to demonstrate feasibility of the information extraction concept. A simple Michelson interferometer was built to simulate operation of the fiber optic gyro. This setup enabled me to concentrate on the extraction concept without getting bogged down in the intricacies of building a fiber gyro.

I would like to express my appreciation to the engineers and technicians at the Frank J. Seiler Research Laboratory for their continuing support of this project, especially Maj Joseph Pollard and MSgt Earl Barr. I am also grateful to my thesis advisor, Maj Salvatore Balsamo, for keeping me on track, and maintaining a positive attitude about the project. Capt Mark Nelson, a fellow thesis student, was also a valuable source of information and encouragement throughout the experiment. Finally, I thank my loving wife, Donna, whose encouragement, patience and hard work at home freed me to work on this thesis.

Daniel J. Brett

List of Figures

<u>Figure</u>		<u>Page</u>
1	Simple Sagnac fiber interferometer	1
2	General block diagram of control loop	4
3	Output intensity vs path length difference	6
4	Amplitude modulation of path length difference	8
5	Sagnac interferometer using fiber length changer for modulation	9
6	Path length difference for a given modulation	10
7	Path length difference with amplitude variation of modulation	10
8	Rotation information	11
9	Intensity change information	13
10	Wavelength change information	14
11	General block diagram of experiment	16
12	Michelson vs Sagnac interferometer	19
13	"Staircase" modulation signal	20
14	Comparison of modulation techniques	21
15	Changing bias of modulation.	23
16	Sample/hold circuit	24
17	Sample/hold output	25
18	Output intensity curve	29
19	Small signal bandwidth test	31
20	Large and small signal bandwidths	32
21	Staircase data points	33

List of Figures

(Continued)

<u>Figure</u>		<u>Page</u>
22	Program flow diagram	35
a	Main program	35
b	Loops A, D, E and F	36
c	Loops B and C	37
d	Compare and control	38
23	Sample/hold output (top trace)	39
24	Feedback signal for a simulated rotation . .	42
a	0.2 Hz	42
b	0.5 Hz	42
c	1 Hz	43
d	5 Hz	43
e	10 Hz	44
f	20 Hz	44
g	30 Hz	45
h	40 Hz	45
i	70 Hz	46
A-1	Sagnac effect	50
B-1	Simple Sagnac interferometer	53
B-2	Phase difference uncertainty	54
B-3	Minimum reciprocal configuration	57
C-1	Photodetector bias circuit	60
C-2	Control loop schematic	62

List of Tables

<u>Table</u>		<u>Page</u>
B-1	Effects causing drift	58
B-2	Effects causing noise	58
B-3	Effects causing scale factor changes	59

ABSTRACT

4
The purpose of this experiment was to determine feasibility of the amplitude modulated dither technique of extracting rotation information from a fiber optic gyroscope. By varying the amplitude of the modulation appropriately, information can be obtained at points on the output intensity curve that are most sensitive to rotation. These points are also in the most linear region of the curve.

A Michelson interferometer is used to simulate a Sagnac interferometer undergoing rotation. A digital control loop processes the information obtained by amplitude modulation and generates a feedback signal to null the path length difference.

The feedback signal is monitored while a rotation simulation signal is introduced to the interferometer. The feedback signal tracks the simulation signal at 180° out of phase (negative feedback). The test setup performs as expected to the hardware and operating frequency limits.

7

I. Introduction

Background

In 1913, G. Sagnac demonstrated that rotation rate could be sensed by measuring a path length difference between counter-rotating light beams traveling a closed optical path (Ref 1:3). This Sagnac effect, derived in Appendix A, is the basis for optical rotation sensing. Optical rotation sensors have advantages over traditional mechanical gyros in that they have no moving parts, very short warm-up time, essentially zero g-sensitivity and light weight.

One form of optical rotation sensor is the fiber optic Sagnac interferometer. This device, described along with some inherent error sources in Appendix B, is shown in simple form in Fig 1. This type of rotation sensor uses optical fiber rather than mirrors to close the optical path.

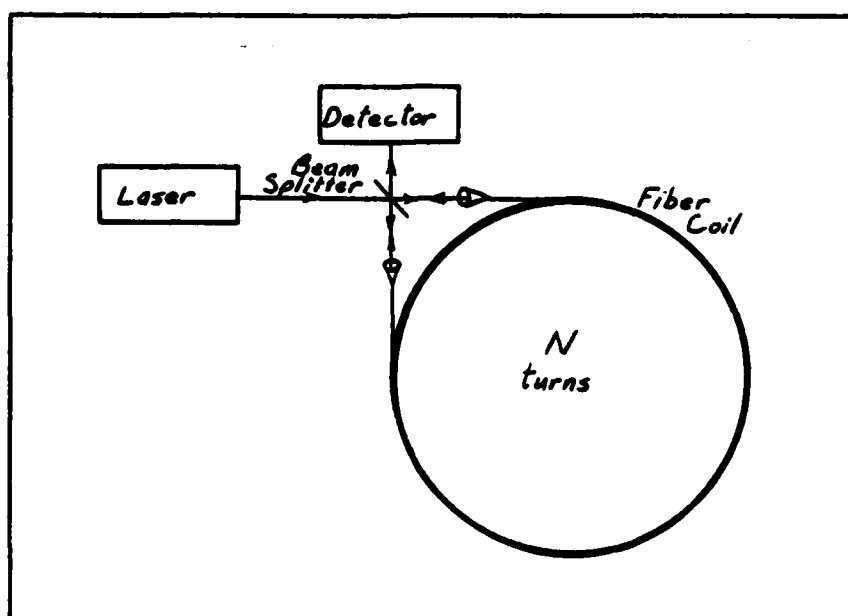


Figure 1. Simple Sagnac fiber interferometer

Several different methods have been proposed for sensing rotation in fiber optic rotation sensors (Ref 2):

(1) Imposing a static 90° phase difference between the clockwise (cw) and counterclockwise (ccw) directions.

(2) Alternating the 90° phase shift.

(3) Phase nulling by propagating slightly different, and variable, frequencies around the loop.

(4) Conveying the phase difference, by heterodyne techniques, to an intermediate frequency and processing it electronically.

This thesis focuses on a technique similar to the phase shift technique described by (2). In addition to alternating a 90° phase shift between the cw and ccw beams, a 270° phase shift is also alternated. Throughout the rest of the paper, phase shifts are referred to as path length differences; they are directly related to each other.

Problem and Scope

The problem is to determine whether the amplitude modulated dither technique is a feasible way of extracting rotation information from a fiber optic Sagnac interferometer.

Due to the complexity involved in building a Sagnac fiber interferometer, this project is limited to showing the feasibility of the amplitude modulated dither technique using a Michelson interferometer. The Michelson interferometer is modified to simulate operation of a Sagnac interferometer. One arm of the Michelson interferometer is used to simulate

modulation of the difference between ccw path lengths, and the other arm is used to simulate rotation of the device. The experiment is set up to show the feasibility of the amplitude modulated dither concept, and is not intended to demonstrate the maximum attainable degree of accuracy.

Assumptions

The testing in this experiment is done at a modulating frequency far below that required for a fiber interferometer (500 Hz vs 150 KHz). This low frequency is due to the operational limits of the piezoelectric transducer (PZT) available for this experiment. It is assumed that success of this experiment at a low frequency shows feasibility of the same method at a much higher frequency in a Sagnac fiber interferometer. This assumption is made because the fiber-wound PZTs suggested for use as modulators for fiber optic gyros (Ref 1:157) operate in the high kilohertz range necessary for that application.

It is also assumed that the Michelson interferometer to be used in this experiment is an adequate model of the Sagnac fiber interferometer insofar as it is used to demonstrate the new rotation information extraction technique. Success of a relatively crude model implies a higher degree of success in the actual fiber interferometer. It must also be assumed that errors introduced by the use of fiber optics do not significantly detract from the new technique. This assumption is possible because the availability of low loss, high

grade, polarization preserving fiber greatly reduces error sources such as birefringence. Also, error sources such as backscattering are reduced by new splicing techniques.

General Approach

A mechanism is required to extract rotation information from the Michelson interferometer. In this case, feedback is employed to control the path length difference sensed by the interferometer when rotation is simulated. This control loop is diagrammed in Fig 2.

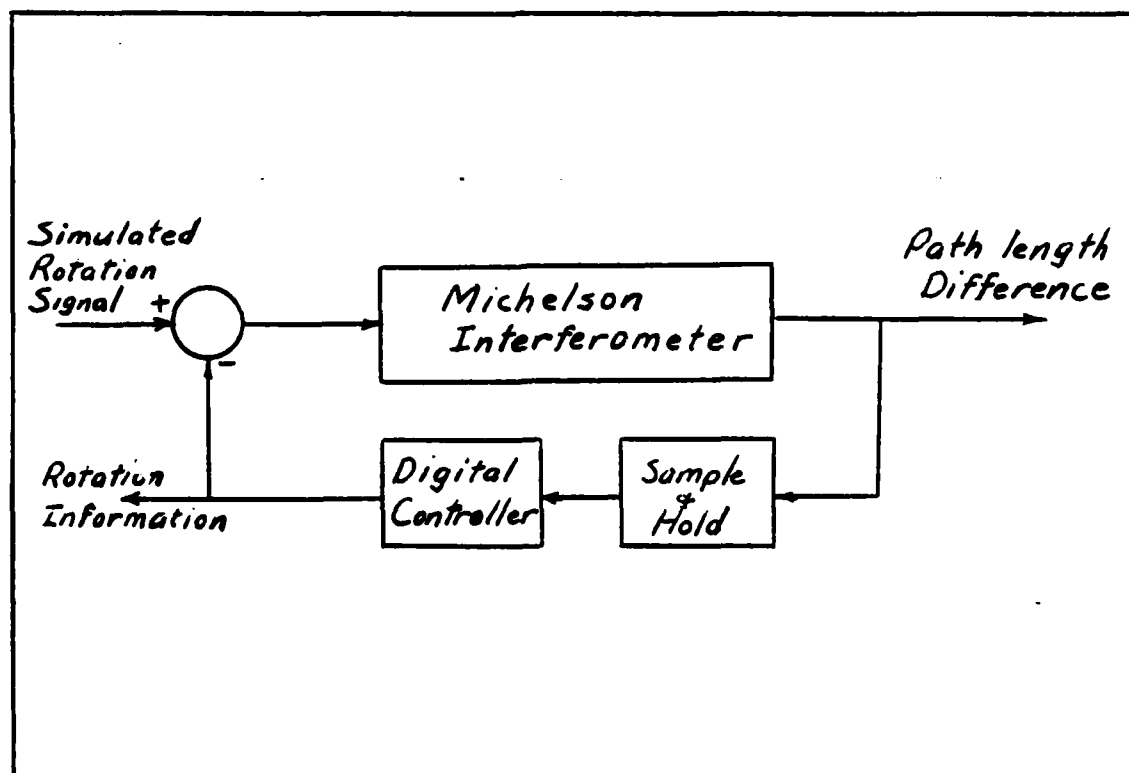


Figure 2. General block diagram of control loop

Essentially, the path length difference Δl is sampled using amplitude modulated dithering of the path length in one arm of the interferometer. A feedback signal proportional to Δl is generated by a digital controller. This feedback signal, while maintaining $\Delta l = 0$, also provides the rotation information desired, because Δl is related to rotation rate Ω by the relationship of Eq (A-3) (developed in Appendix A).

Sequence of Presentation

First of all, the method of extracting rotation information using amplitude modulation is described theoretically. The modulation signal, the data sampled, and the conversion of that data into useful information are also discussed in this section on theory.

Following a general description of the feedback control loop, implementation of each individual function of the loop is explained. The components to be described are the Michelson interferometer, the sample and hold (S/H) circuit, analog to digital (A/D) and digital to analog (D/A) converters, and the digital computer.

Finally, the experimentation procedure is examined, including determination of hardware limits and operating points, software development, and collection of data. Analysis of the data yields results, from which conclusions are drawn concerning feasibility of the method, and recommendations are made regarding further development of the technique.

II. Theory

Method of Amplitude Modulation

The basic premise of a fiber optic rotation sensor is that rotation rate can be measured by obtaining the path length difference of counter-rotating beams of light. This path length difference can be related directly to a corresponding change in the output intensity of the rotation sensor (in this case, a Sagnac fiber interferometer). Fig 3 shows that the greatest sensitivity to path length changes occurs at the points of maximum slope ($\pm \lambda/4, \pm 3\lambda/4$). The peaks and minimums of the output intensity curve correspond to completely constructive and destructive interference, respectively.

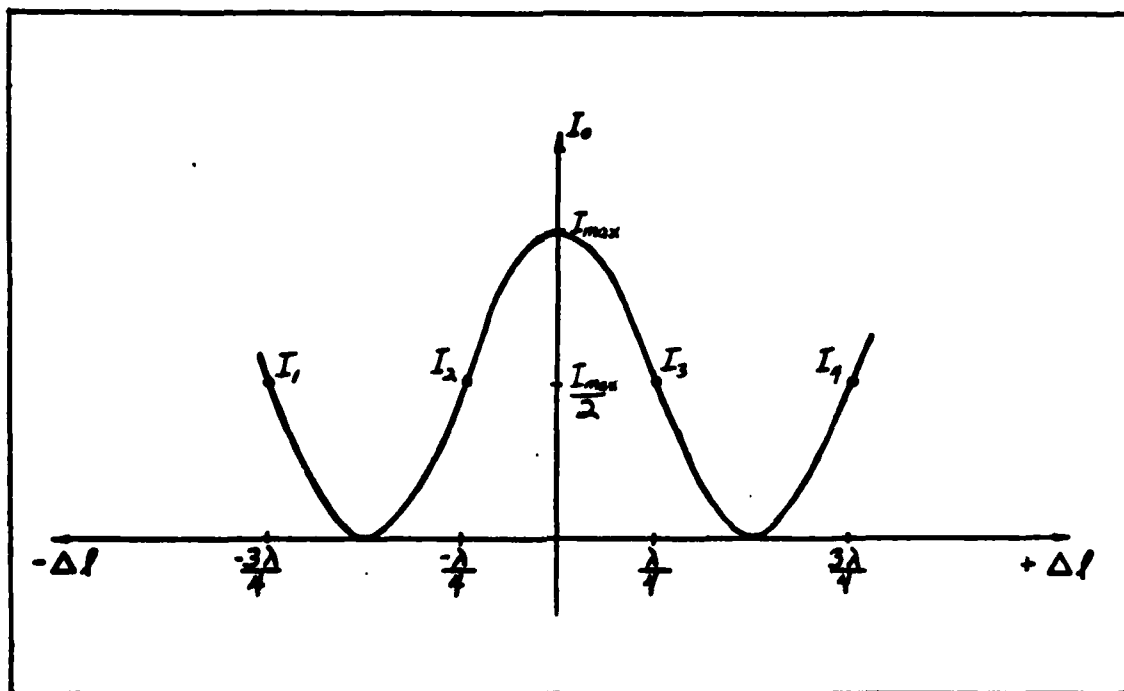


Figure 3. Output intensity vs path length difference

The ideal points at which to collect rotation information are the points of maximum slope (I_1, I_2, I_3 and I_4), not only from the standpoint of maximum sensitivity, but also because of the approximate linearity of these regions. A method of doing this is to amplitude modulate the path length difference of the interferometer in order to be operating in these linear regions, as shown in Fig 4.

Assuming no rotation of the device, the modulation signal modulates the path length difference to the four points of maximum slope shown in Fig 4 (I_3, I_2, I_4 and I_1). This can be physically accomplished by placing some type of fiber length changer close to one end of the Sagnac interferometer fiber loop as shown in Fig 5. This fiber length changer (i.e., a fiber-wound PZT) changes the length of the fiber loop by ΔL when a voltage V is applied. If the length of the fiber loop is L_1 when no voltage is applied to the fiber length changer, then when the voltage V is applied, the loop length becomes

$$L_1 + \Delta L = L_2$$

It is assumed that $L_1 = 1$ km, $\Delta L \ll 1$ km and the PZT is placed very close to the beam splitter. It is also assumed that the PZT changes size instantaneously as voltage is applied. Consider two photons, each starting at the beam splitter at time t_0 and traveling in opposite directions. If no voltage is applied at t_0 , and the voltage V is applied

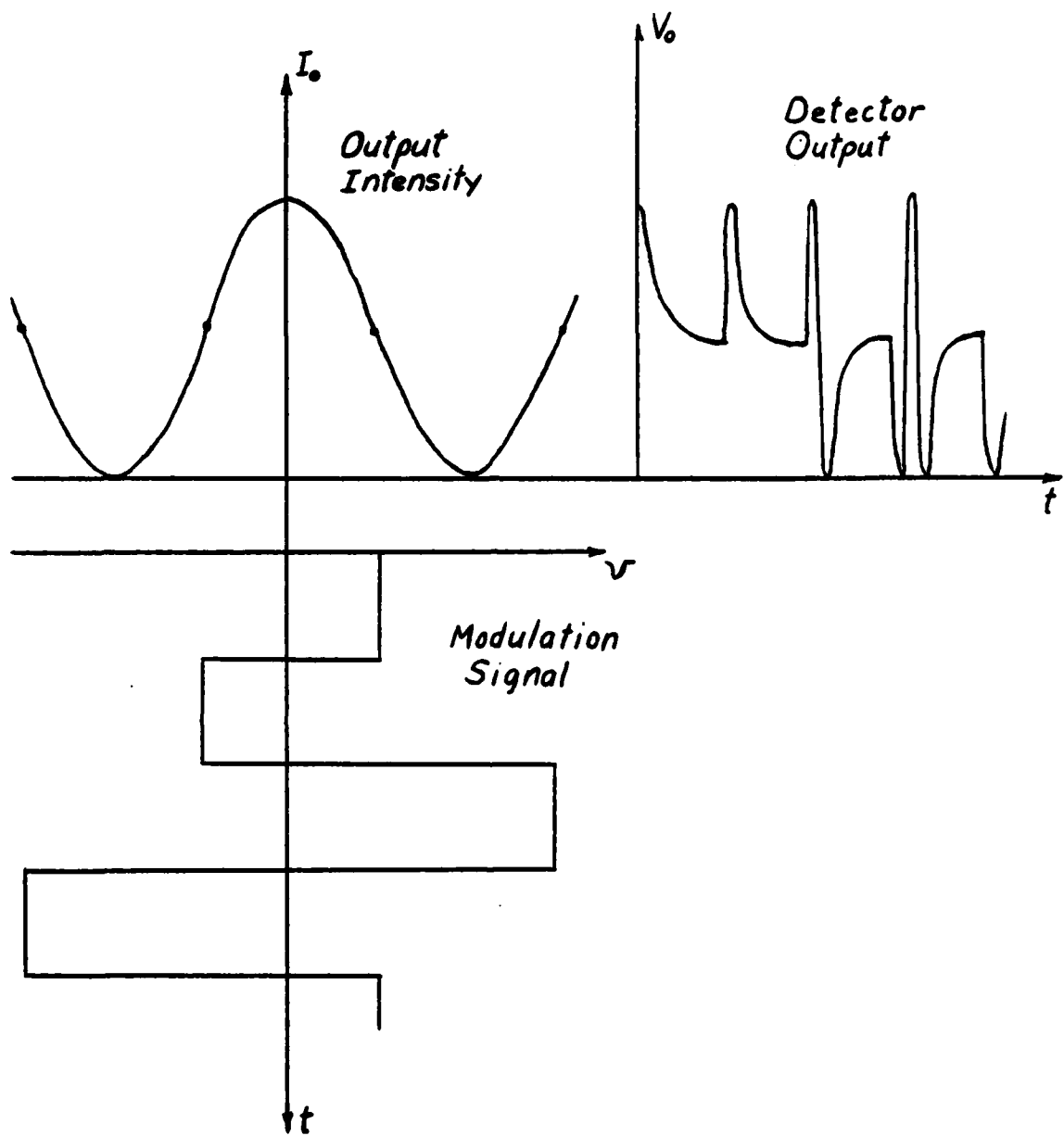


Figure 4. Amplitude modulation of path length difference

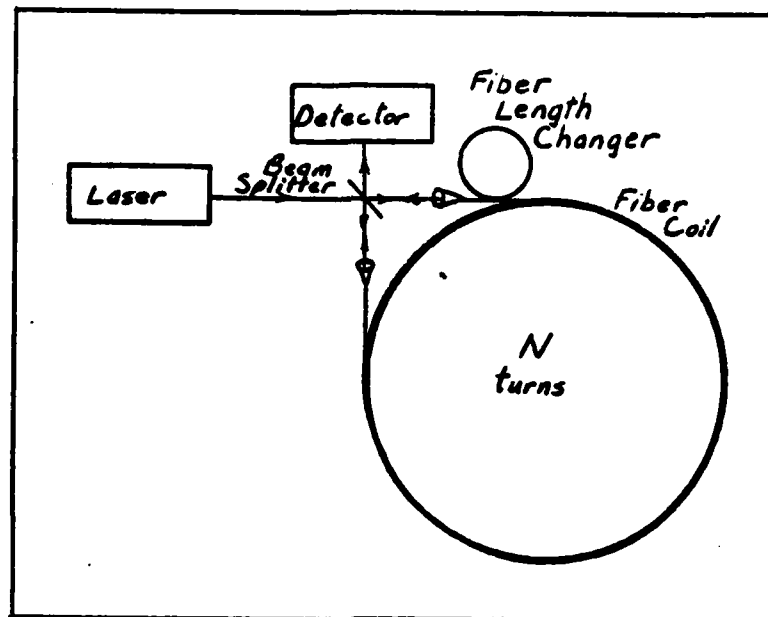


Figure 5. Sagnac interferometer using fiber length changer for modulation

right before the ccw photon reaches the fiber length changer, the ccw photon travels a length L_2 to complete the loop, while the cw photon only has to travel a length L_1 . Assume the path length changer is modulated between 0 volts and V volts at a frequency whose half period coincides with the round trip time of light through the loop. Then the resultant path length difference is shown by Fig 6.

Assuming that the fiber length changer operates linearly in the region of interest, a modulation signal such as that shown in Fig 4 can be obtained with the PZT input shown in Fig 7. By modulating the path length difference in this manner, the interferometer is as sensitive as possible to rate of rotation because information is being collected around the points of maximum slope.

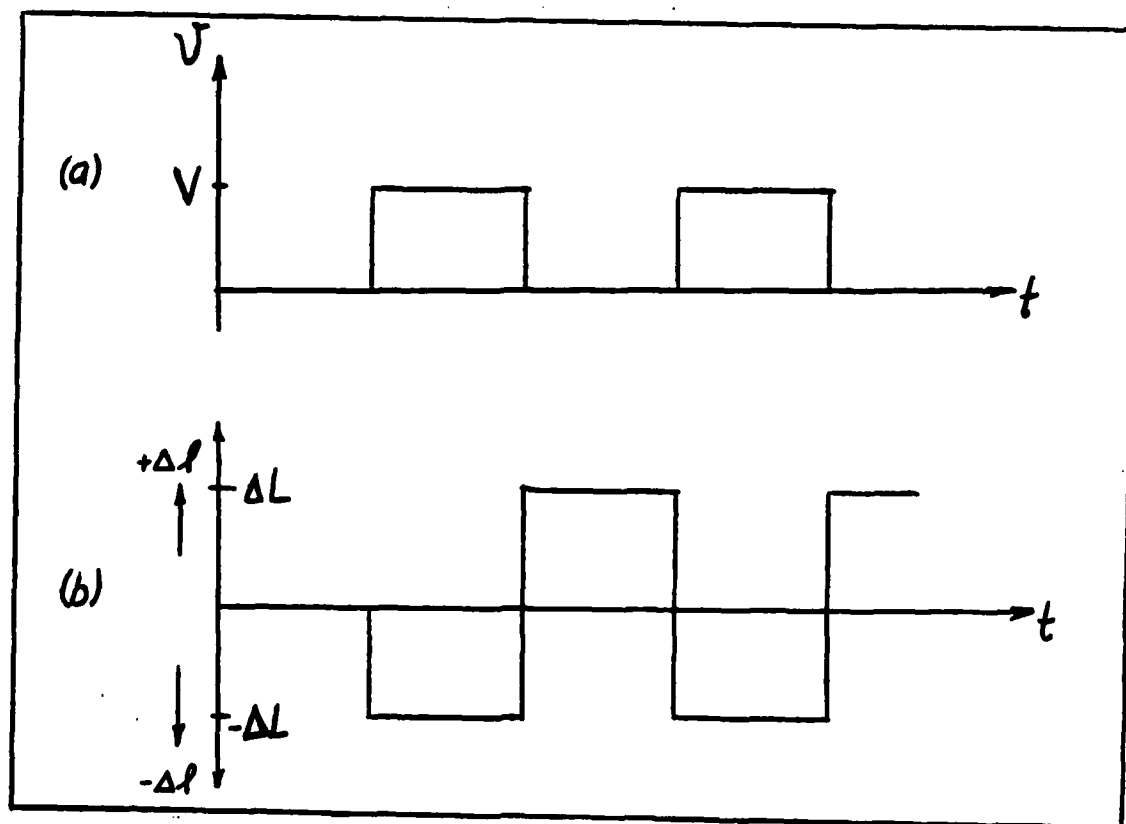


Figure 6. Path length difference (b) for a given modulation (a)

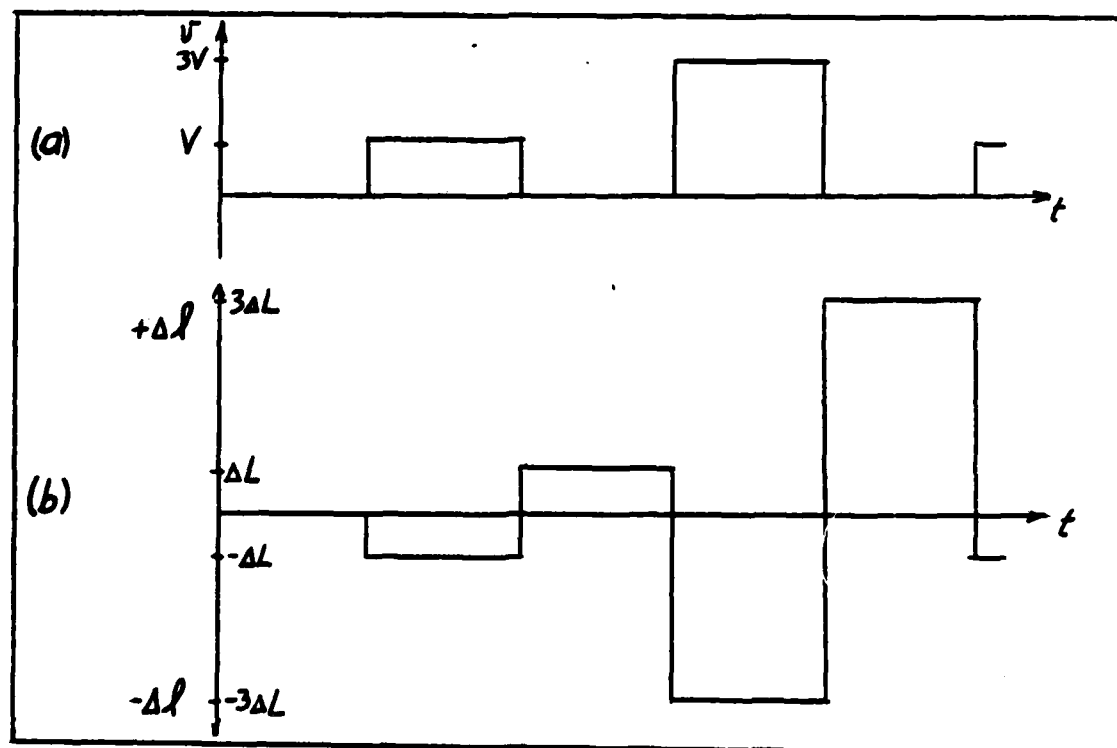


Figure 7. Path length difference (b) with amplitude variation of modulation (a)

Significance of Data Obtained

Basically, three types of useful data can be obtained using this extraction technique. First of all, the primary purpose of the Sagnac interferometer is to detect rotation rate. In open-loop operation, rotation can be sensed by detecting deviations from the half maximum values I_1, I_2, I_3 and I_4 , as shown in Fig 8. By sampling the values of output intensity at these four points, and calculating

$$(I_1' + I_3') - (I_2' + I_4') = \Delta I_0 \quad (1)$$

a value proportional to rotation rate is available. Once the relationship between I_0 and ΔI is experimentally determined,

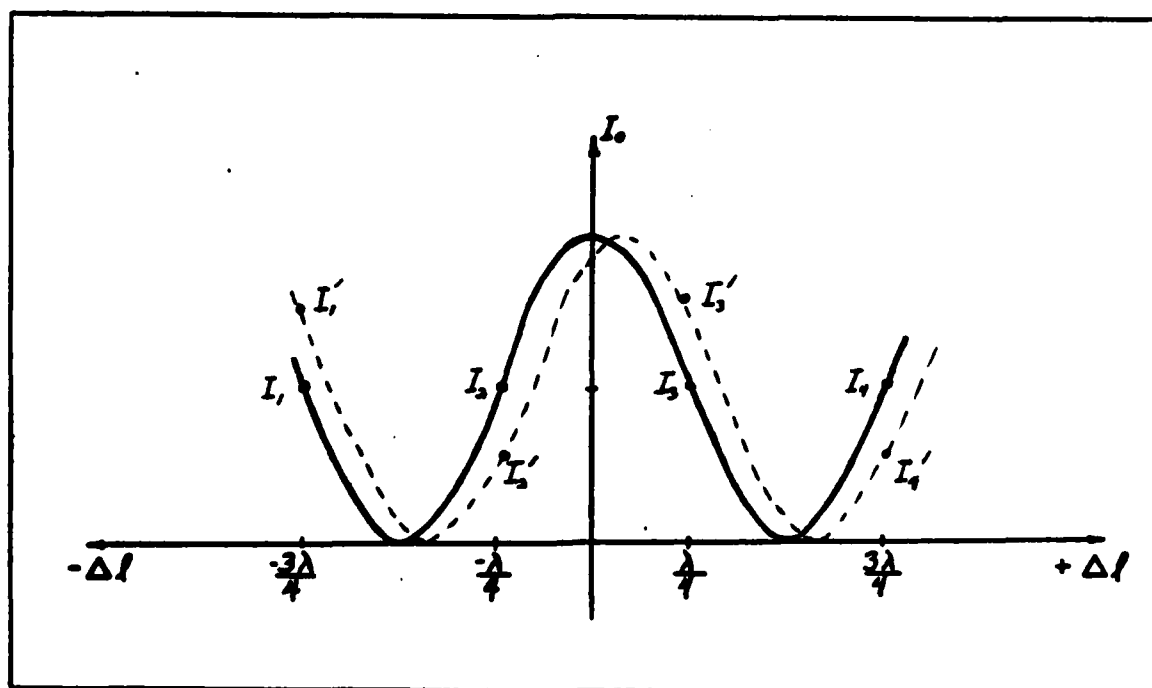


Figure 8. Rotation information

rate of rotation is found using the relationship

$$\Delta l = \frac{4\pi R^2 N}{c} \Omega \quad (2)$$

where

R = radius of fiber loop

N = number of turns of loop

c = speed of light

Ω = rate of rotation

(See Appendix A for derivation) The direction of rotation depends on the sign of ΔI_0 .

Changes in intensity of the light source may also be detected using these data. Fig 9 shows how an intensity fluctuation can affect the output intensity curve. It can be seen in this case that

$$\frac{I_1' + I_2' + I_3' + I_4'}{2} = I_D + \Delta I_D \quad (3)$$

where

I_D = desired maximum intensity

ΔI_D = deviation of intensity from desired value

The calculated deviation of intensity can be used as a

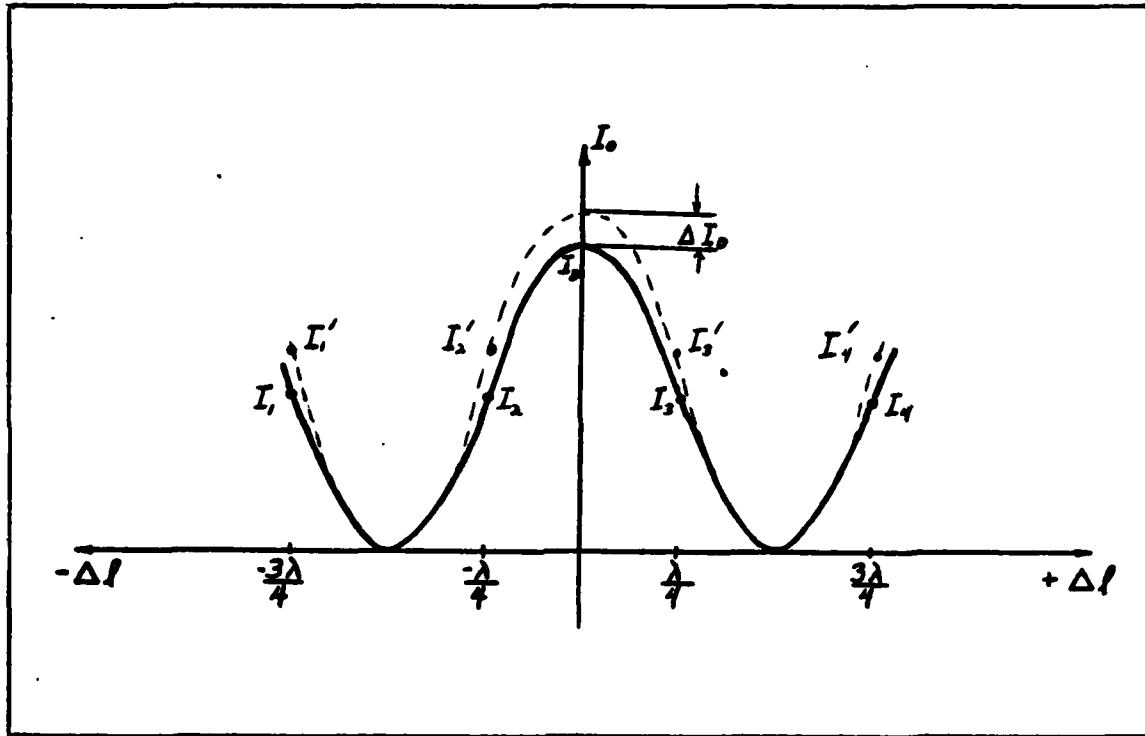


Figure 9. Intensity change information

feedback signal to stabilize the intensity of the light entering the interferometer.

A third calculation that can be used from this configuration is a change in the wavelength of the light entering the interferometer. Fig 10 shows that fluctuation in wavelength can be approximated to first order by

$$(I_2' + I_3') - (I_1' + I_4') = k\Delta\lambda \quad (4)$$

where

k = experimentally determined constant

$\Delta\lambda$ = change in wavelength

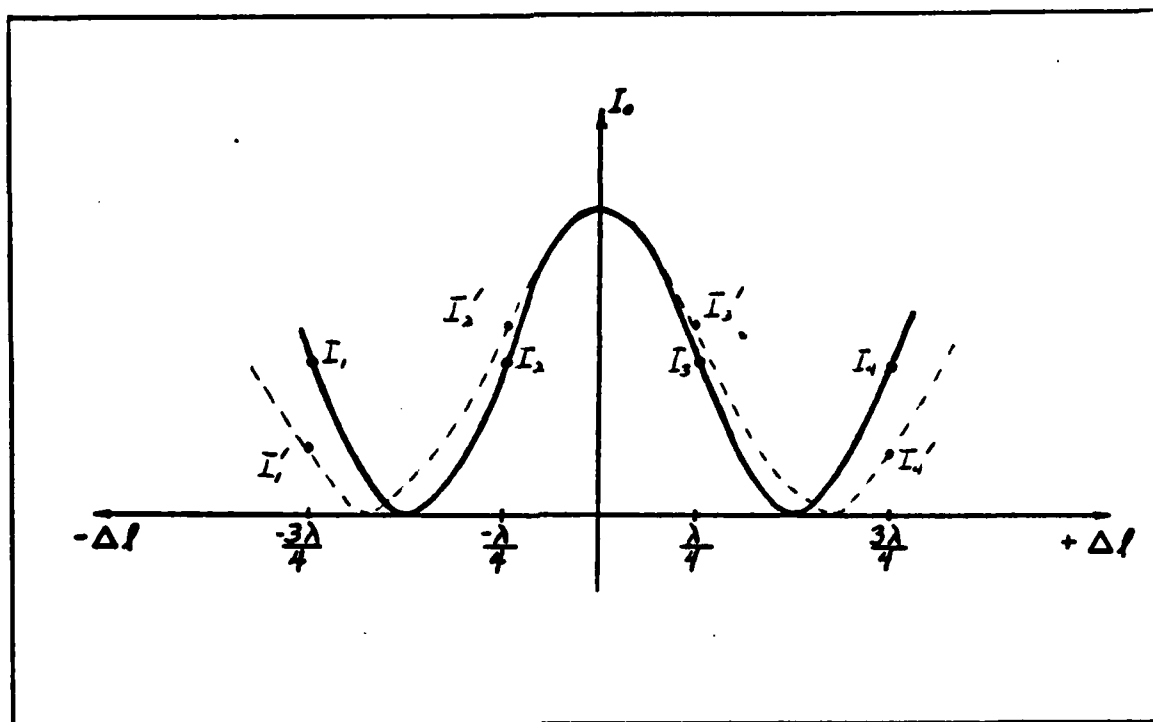


Figure 10. Wavelength change information

This deviation from the desired wavelength, $\Delta\lambda$, can be useful as feedback for controlling the wavelength of the light entering the interferometer, or at least accounting for the change in wavelength.

It must be pointed out that a fluctuation in any of the three parameters (rotation, intensity and wavelength) is assumed to be limited to the approximately linear regions of the output intensity curve. This assumption imposes some limits on the rotation rate to be measured. Maximum $\Delta\lambda$ that can be detected fairly linearly is $\pm \frac{\lambda}{4}$.

Assuming

$$\lambda = 633 \times 10^{-9} \text{ meters (HeNe laser)}$$

$$c = 3 \times 10^8 \text{ meters/sec}$$

$$\pi R^2 N = A_{\text{eff}} = \frac{10^6}{4\pi} \text{ meters}^2 \text{ (1 km fiber loop)}$$

where

A_{eff} = effective area enclosed by fiber loop

then

$$\Omega_{\text{max}} = .6 \times 10^{-3} \text{ rad/sec} \quad (5)$$

General Layout of System

For the purpose of this experiment, fluctuations in intensity and wavelength of the light source are ignored. The parameter of interest is rate of rotation. The block diagram of Fig 11 gives the general design of the system which obtains the rotation information.

This system is actually a control loop which keeps the maximum point of the output intensity of the interferometer centered on $\Delta I = 0$ (See Fig 3). The feedback signal is inversely proportional to the induced rate of rotation and provides the rotation information that is desired.

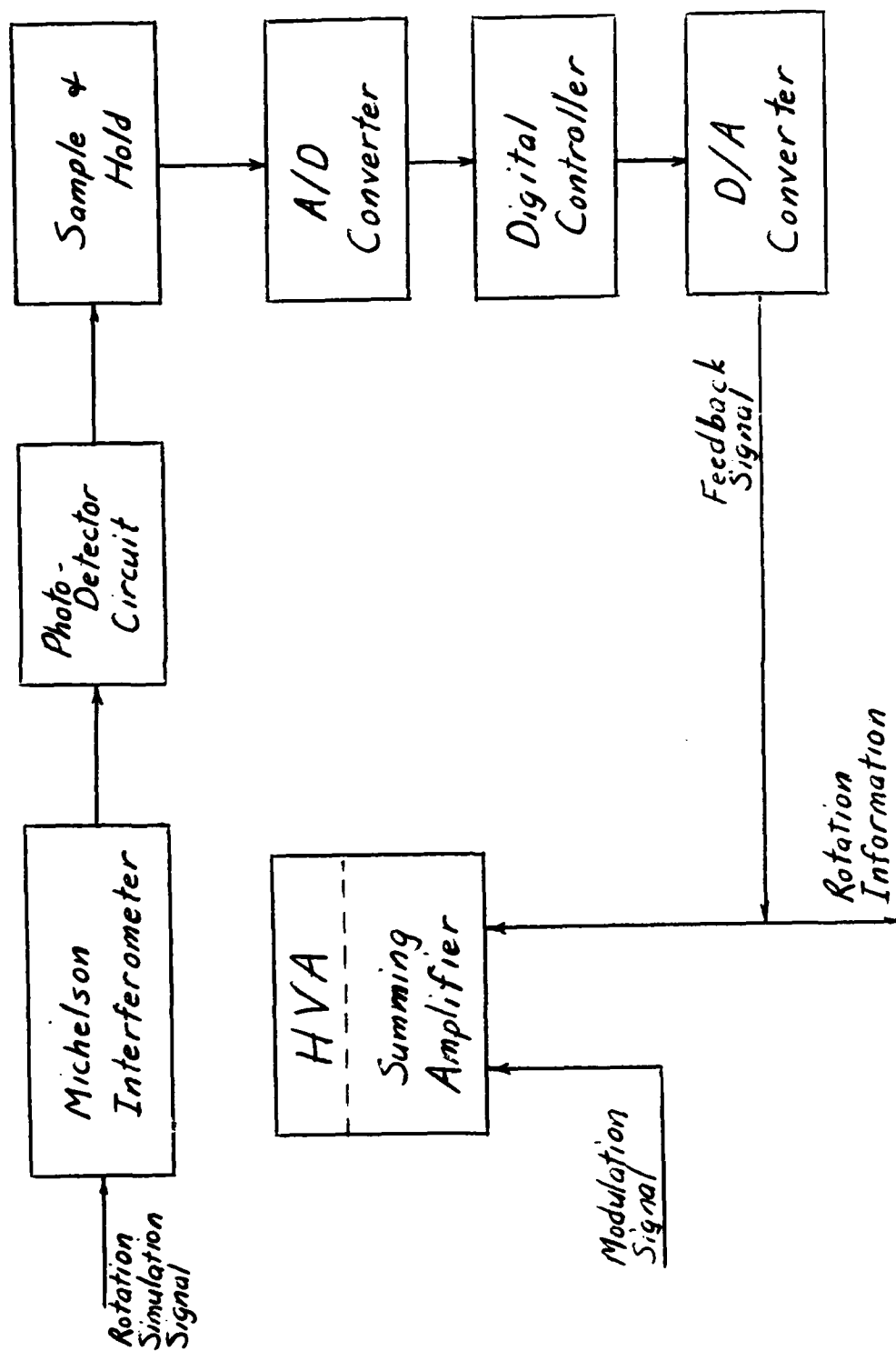


Figure 11. General block diagram of experiment

The feedback control signal is generated by a digital computer. The computer takes samples of the interferometer output intensity, performs the calculation of Eq (1), and feeds back a proportional control signal which changes the bias of the amplitude modulation signal and drives the maximum intensity point back toward $\Delta\ell = 0$. The feedback signal should exactly follow the rotation simulation signal, but is 180° out of phase.

Before getting into the details of the experimental setup, note that a digital computer is being used as a controller as opposed to a hardwired digital circuit. This allows the flexibility desired for experimental work.

III. Experimental Setup

Introduction

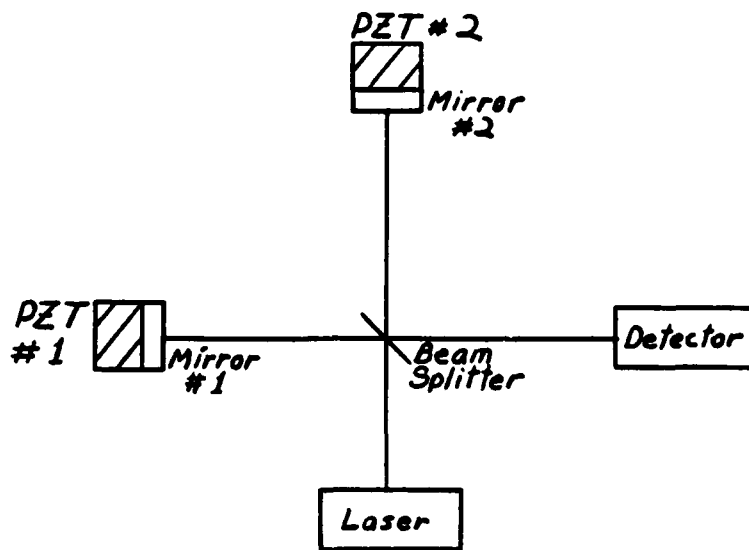
Since a digital computer is being used as the controller, the experimental setup involves a blend of hardware and software. This section focuses on the hardware development of the system, taking each block of Fig 11 and expanding on it. A detailed circuit of the entire control loop appears in Appendix C.

Michelson Interferometer and Photodetector

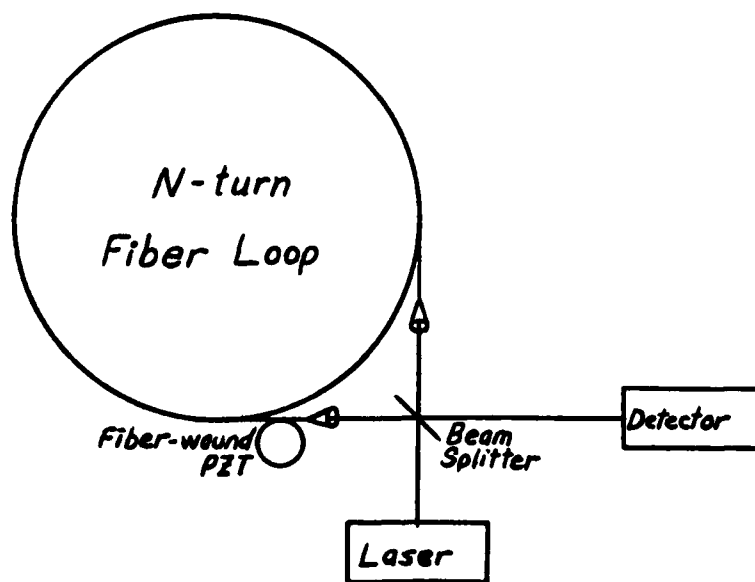
In Chapter I, it is assumed that a Michelson interferometer adequately simulates the operation of a Sagnac interferometer for the feasibility demonstration of this experiment. The configuration in Fig 12 shows how this simulation is accomplished. Using a Michelson interferometer for the experiment rather than a Sagnac fiber interferometer avoids the high precision required to get light into an optical fiber while still effectively demonstrating the feasibility of the data extraction method.

Referring to Fig 12, it can be seen in (a) that the reflection of light off mirror #2 simulates the cw direction of the light in (b). Using this fact, the path length of the cw traveling light can be changed by moving mirror #2 with PZT #2.

Also in Fig 12, it is observed that reflection of light off mirror #1 in (a) is analogous to light traveling in the



(a) Michelson interferometer



(b) Sagnac fiber interferometer

Figure 12. Michelson vs Sagnac interferometer

ccw direction in (b). The desired modulation of the fiber can be simulated by modulating mirror #1 with PZT #1. This is done by directly modulating PZT #1 with the signal shown in Fig 13.

This modulating signal is different than the signal shown in Fig 7(b). Due to the time constant introduced when driving a PZT (capacitive load), it is found experimentally that the PZT has more time to react to the "staircase" signal in Fig 13. As shown in Fig 14(a), the extreme voltage swings of the other signal cannot be accomplished at 500 Hz with the power limitations of the equipment available for this experiment.

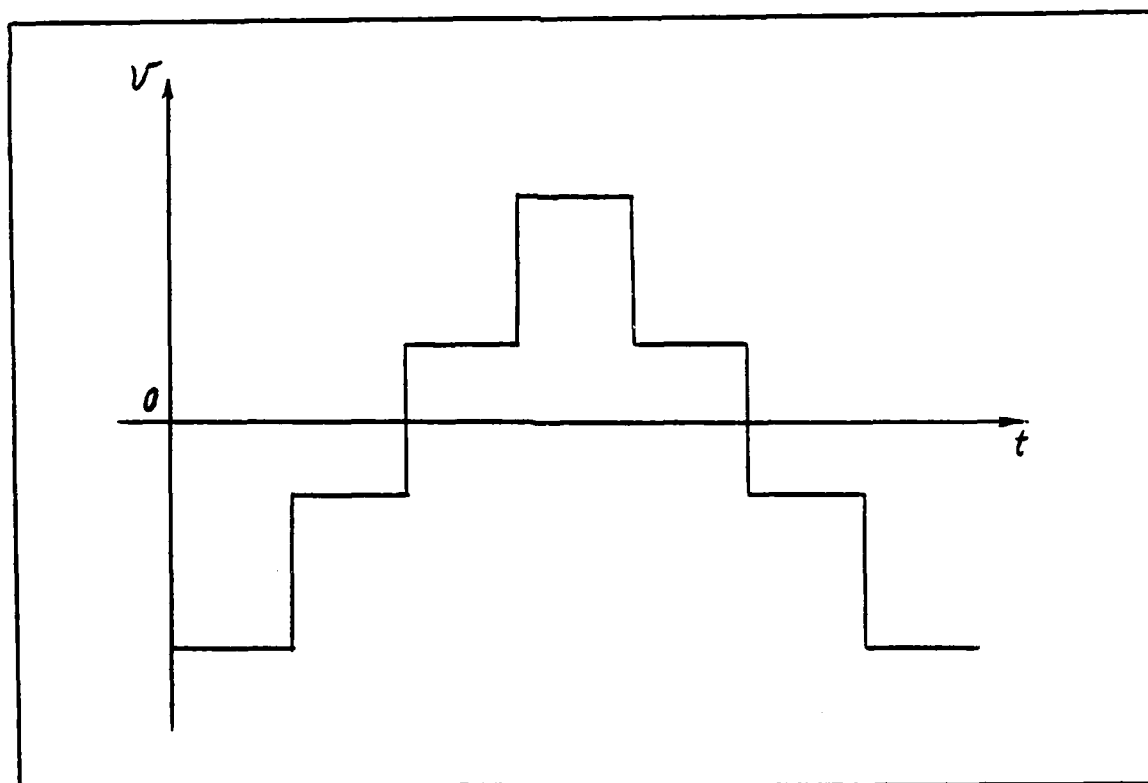
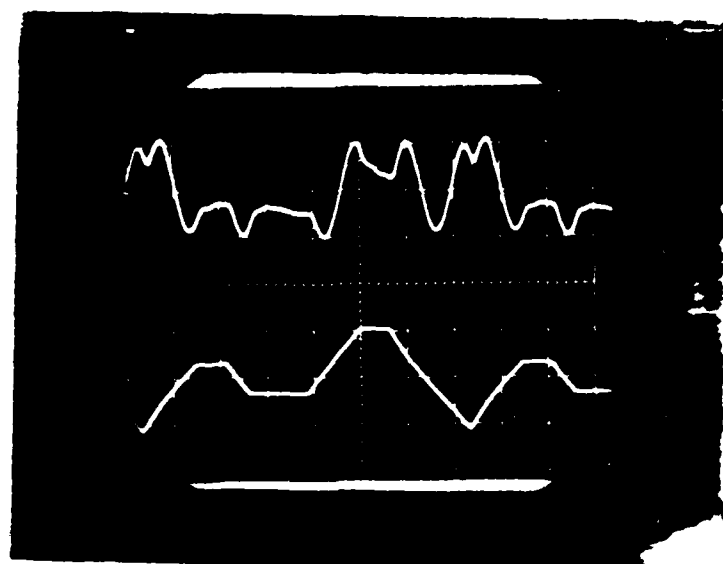
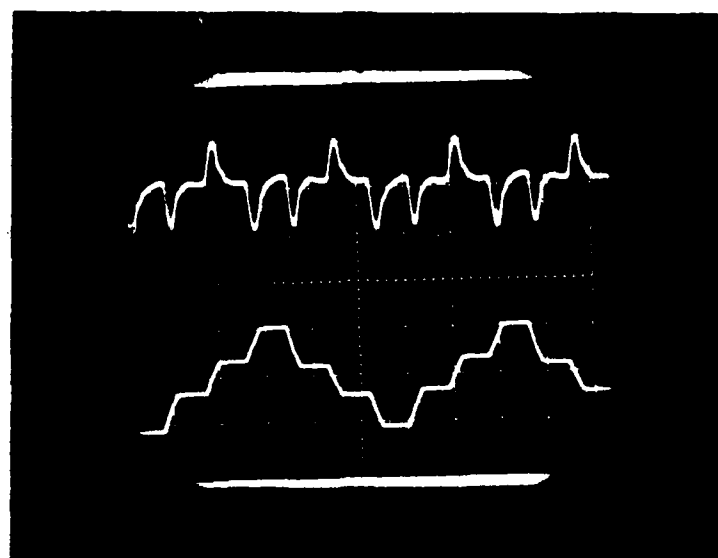


Figure 13. "Staircase" modulation signal



(a) Extreme swing



(b) Staircase

Figure 14. Comparison of modulation techniques

Using the staircase modulation approach, the photodetector output appears as in the upper trace of 14(b). The diagram of Fig 15 illustrates how the photodetector output is used to generate a feedback signal which drives Δl back to zero. First, a rotation is induced, causing a positive path length difference. The magnitude of this path length difference is proportional to the result of Eq (1), or

$$(I_1' + I_3') - (I_2' + I_4') = \Delta I_0$$

Once the proportionality between ΔI_0 and Δl is determined experimentally, an appropriate feedback signal to PZT #1 drives Δl of the interferometer back toward zero. It can be seen from the modulation signal in Fig 15 that this is done by changing the bias of the modulation signal.

The levels used for computation in Eq (1) are obtained from the photodetector output, which is a voltage signal proportional to incident light. Before a digital computation can be performed, the analog voltage must be converted to digital representation. This function is performed by a combination S/H and A/D converter.

S/H Circuit and A/D Converter

The voltage output of the photodetector is fed into a S/H circuit and A/D converter. The end product of this part of the circuit is an 8-bit digital number for each of the voltage levels proportional to I_1, I_2, I_3 and I_4 .

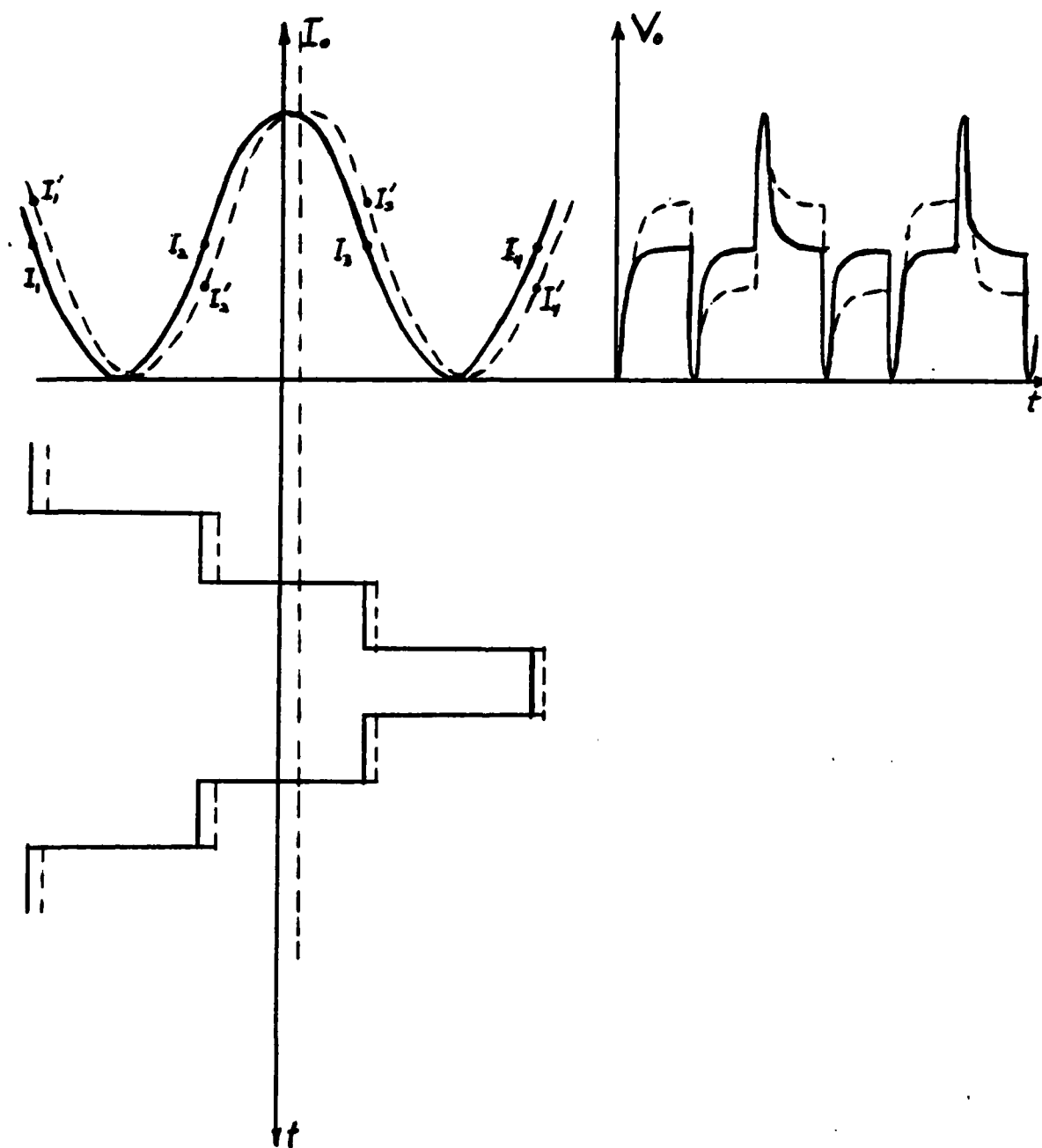


Figure 15. Changing bias of modulation

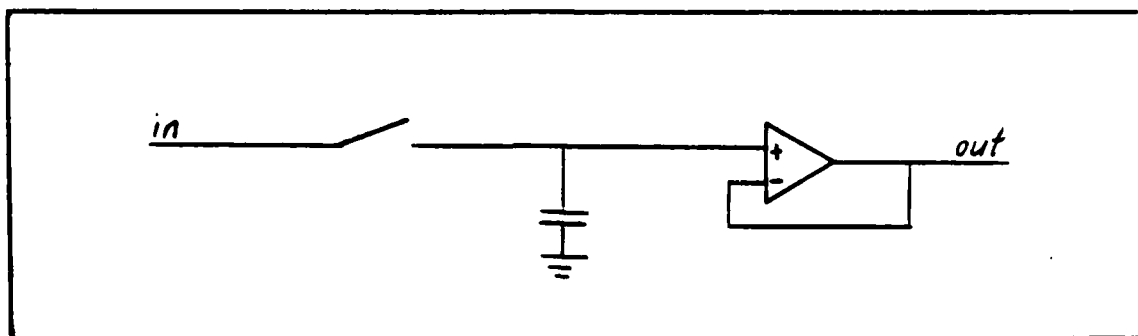


Figure 16. Sample/hold circuit

The S/H circuit consists of a bilateral switch, a capacitor, and an operational amplifier (op-amp) in the configuration of Fig 16. When the switch is closed, the output of the S/H circuit follows the input. When the switch is opened, the final value of the input before opening the switch is held on the output.

The desired portion of the photodetector output occurs right before the modulation signal changes levels, where the PZT response has had time to flatten out and ΔI is at the desired value. A typical output of the S/H circuit is shown in Fig 17, where the S/H output is the middle trace. The bottom trace shows the modulation signal, while the top trace is the actual photodetector output. In this case, the signal is being sampled for the last fourth of each modulation level, then held till the next sample is to be taken. The 7KHz signal superimposed on the photodetector output is related to the resonant frequency of the PZT.

When the S/H circuit is holding a constant value on its output, the A/D converter is able to convert the signal to

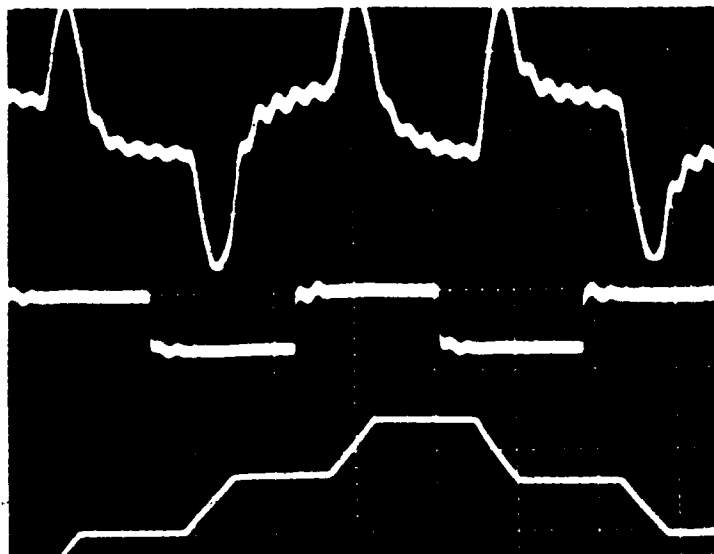


Figure 17. Sample/hold output

an 8-bit representation. This digital number is then available to the computer through an input port. The computer can then manipulate the number as necessary.

Digital Computer and D/A Converter

The digital computer is that part of the control loop which enables the hardware to perform its function. For this experiment, it not only performs the calculations necessary to provide a feedback signal, but also generates the "staircase" modulation signal for PZT #1. Additionally, it triggers the S/H and A/D converter with logic enable signals when necessary.

The computer is an 8080-based microprocessor designed and built at the Frank J. Seiler Research Laboratory. The

data input/output provisions for the computer include four programmable input/output ports for interfacing with and controlling the A/D converter and two D/A converters. One D/A converter is dedicated to generating the amplitude modulation signal. The other D/A converter provides the feedback control signal.

Summing and High Voltage Amplifiers

The final stage in the loop has the two-fold function of algebraically adding two signals and amplifying the resultant signal. The feedback signal is added to the digitally generated modulation signal. The high voltage amplifier (HVA) is required, finally, to amplify the voltage level of the PZT input to an acceptable level. In this case, the HVA is set up for a gain of ten so that, for an input between ± 5 V, the output is ± 50 V. This voltage is needed to move the PZT's mirror sufficiently to hit all four operating points.

Summary

The overall function of the loop is to provide path length control for the interferometer. This control is accomplished by sampling the photodetector output, computing path length difference, and introducing a proportional feedback signal to PZT #1.

IV. Test Procedure

Introduction

Testing of the effectiveness of the control loop is accomplished by introducing a known signal to simulate rotation and observing the feedback signal. First, the interferometer is aligned till an appropriate interference pattern is observed at the output. Then, the required amplitudes of modulation are determined experimentally. Third, the limits of the hardware are determined to find a reasonable modulation frequency for experimentation. Last, the test software is developed and test data are collected.

Interferometer Alignment

Alignment of the Michelson interferometer is essential for an interference of the two beams to occur. First, the beam out of the laser is leveled with respect to the interferometer mounting platform. Then the beam in each leg of the interferometer is independently aligned by adjusting its respective mirror. Each mirror is adjustable about its vertical and horizontal axes (two degrees of freedom). When each beam is aligned, the two beams are allowed to interfere while the interference pattern is observed on a piece of paper. The mirror adjustments are then fine tuned to produce a round bright dot in the center of the pattern, indicating totally constructive interference. The fine tuning is continued until completely constructive and destructive

interference is observed while varying the voltage on only one of the PZTs.

Determination of Operating Points

The requirement of this data extraction technique is to modulate PZT #1 to four points on the output intensity curve as shown in Fig 15. It is necessary to determine what amplitude values the modulation signal must have in order to reach these four points. To do this, the output of a function generator, amplified through the HVA, is applied to the PZT to be modulated. A slow ramp function is applied by generating a triangular wave at 0.5 Hz. The resultant output intensity curve is shown in Fig 18.

Since the modulation signal is generated digitally, the analog voltage levels are converted to digital levels. The D/A converter puts out 10 V peak to peak and the HVA is set up for a gain of 10. The maximum output voltage is 100 V peak to peak, or ± 50 V. The maximum intensity point of the curve can be centered on 0 V by biasing one of the PZTs. Since the D/A converter is 8 bits, 0 V is represented by the decimal number 128, or 80 hexadecimal (80H). There are 2^8 , or 256, digital levels, equating to

$$\frac{100 \text{ V}}{256 \text{ levels}} = 0.4 \text{ V/level}$$

Using this value, the digital levels for the modulation signal are calculated. The output intensity curve of Fig 18

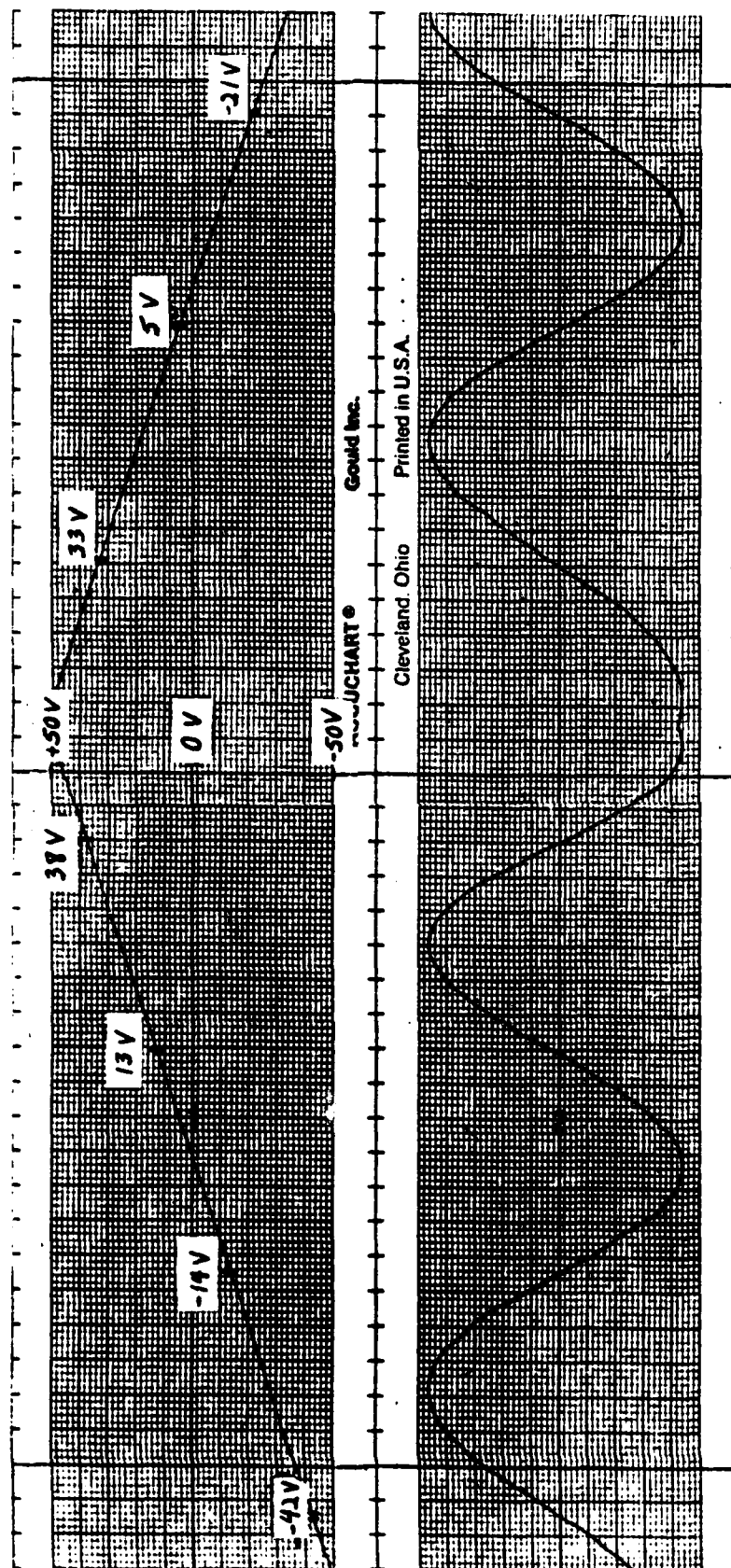


Figure 18. Output intensity curve

shows, however, that the voltage levels on the downward slope of the input to PZT #1 are different than on the upward slope, indicating some hysteresis. This implies that the voltage levels on the "down" side of the staircase differ from those on the "up" side. This matter is addressed in the software development.

Hardware Limits

To determine the experimental operating frequency of the modulation signal, it is important to know the frequency response of the PZT driving system. Both small signal bandwidth and large signal bandwidth are obtained, and 500 Hz is chosen as the modulation frequency for testing because it is well within the bandwidth limitations.

Small signal bandwidth is obtained by modulating in the linear region of the intensity output curve as shown in Fig 19. Large signal bandwidth is plotted by modulating between -50 V and +50 V, or the maximum voltages to which the PZT is driven. Both plots appear together on Fig 20, and show that 500 Hz is a "safe" frequency at which to be modulating.

Software Development

Several functions are to be accomplished by the software. First, the modulation signal is generated digitally. Also, the program must enable the S/H circuit and the A/D converter at the correct times. Last, the software must manipulate data and do the computations necessary to generate

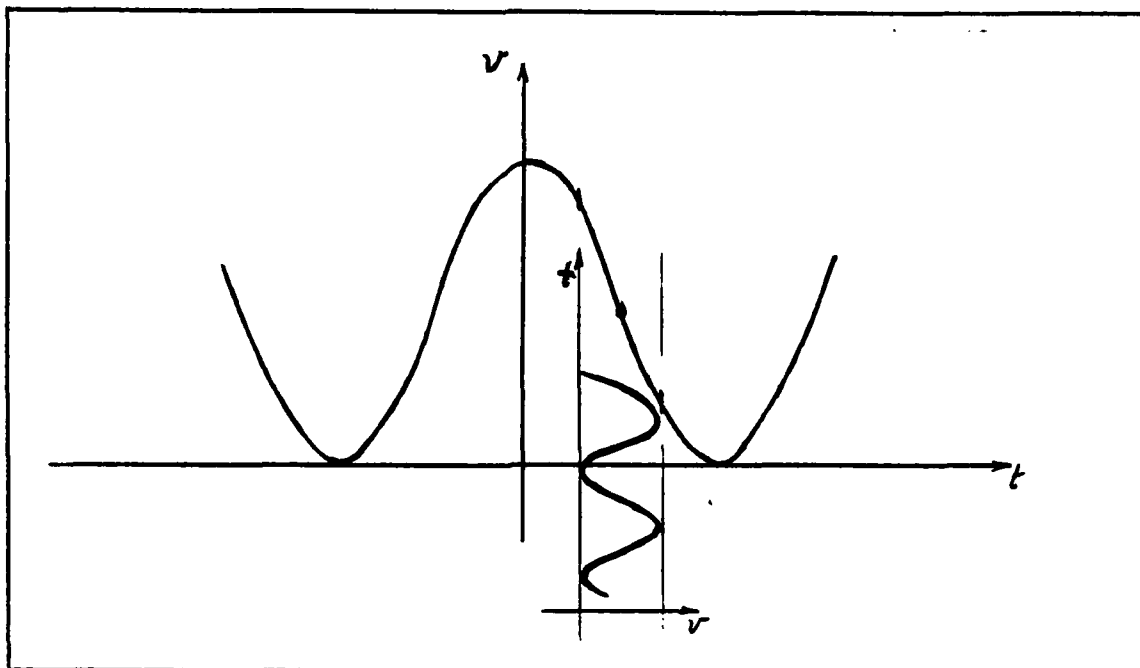


Figure 19. Small signal bandwidth test

a feedback control signal.

The two primary concerns in generating the modulation signal are correctness of the voltage levels and timing. Since the computer has a 4 MHz clock, one machine state is 250 nsec long. The time spent on each voltage level of the modulation signal is $\frac{1}{2}$ cycle, or

$$\frac{T}{2} = \frac{1}{2f} = 1 \text{ msec}$$

$$\frac{1 \text{ msec}}{250 \text{ nsec/state}} = 4000 \text{ machine states}$$

So each $\frac{1}{2}$ cycle is made up of 4000 machine states.

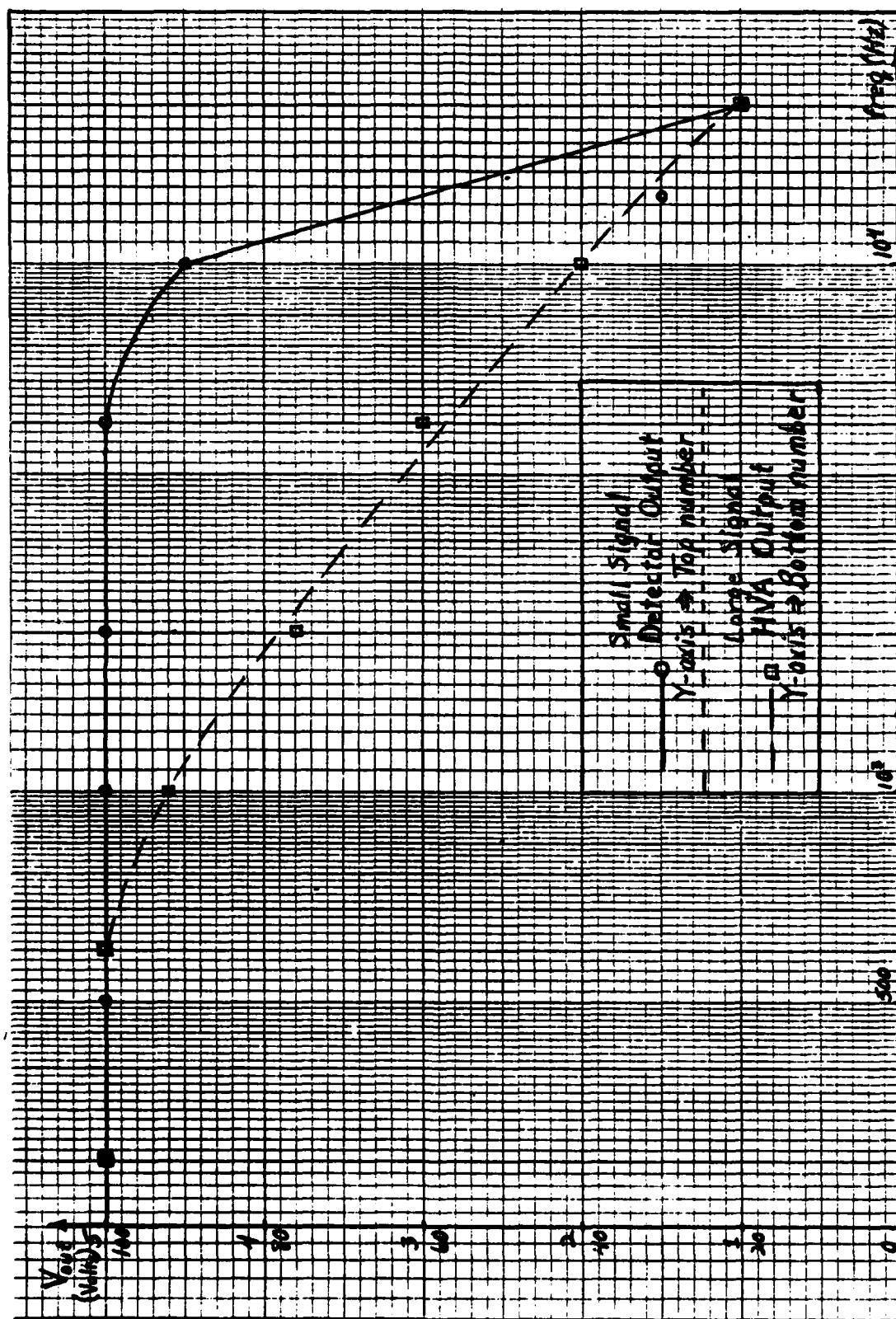


Figure 20. Large and small signal bandwidths

The program enables the S/H circuit for the last $\frac{1}{4}$ of the duration of each voltage level. Right before the voltage level is changed, the S/H circuit is disabled, holding the final value of the photodetector output in that $\frac{1}{4}$ cycle. As soon as the voltage level is changed, the A/D converter is enabled to convert the sampled photodetector output to a digital number. The cycle continues in this manner.

In between A/D conversion and sampling the output, there are over 2000 states available to do computation. The program uses some of these states to keep running totals of the data collected at the four points 1, 2, 3 and 4 in Fig 21. The data collected at points 1 and 4 are added twice for timing purposes. For example, after one time through the staircase (the six levels shown in Fig 21), each data point has contributed two pieces of data to its running total.

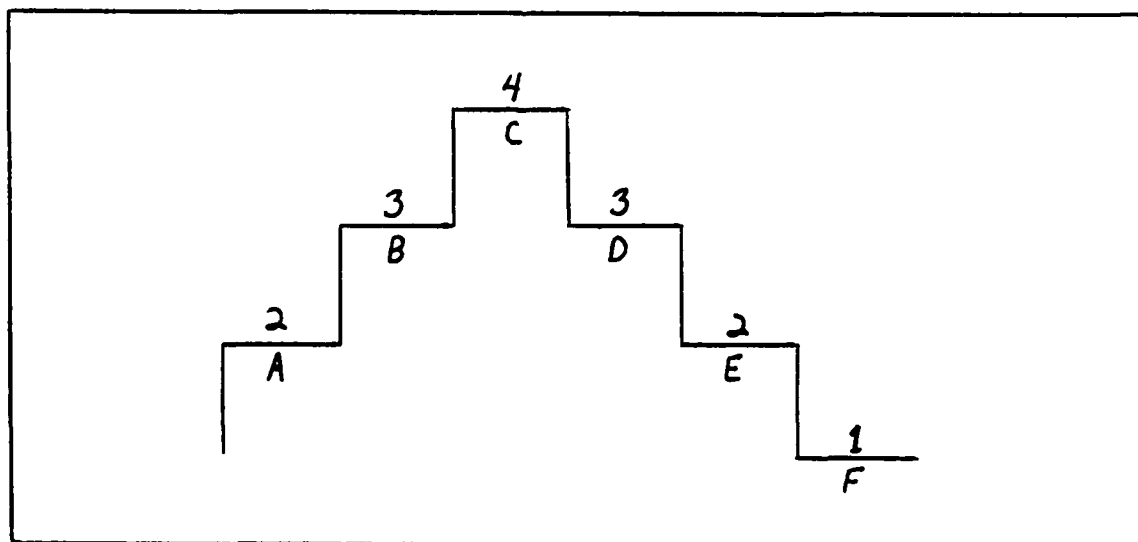


Figure 21. Staircase data points

The program averages each of the totals when specified. Once the totals are averaged, the computation is accomplished and an appropriate feedback signal is generated from the program. Fig 22 shows the flow chart for this program. The assembly language program is located in Appendix D.

Data Collecting

Once the program is up and running, the digital voltage levels are fine tuned to insure modulation to the proper operating points. This is done by finding the maximum and minimum outputs of the photodetector. Then the voltage levels are adjusted till the sampled photodetector outputs can be brought into a reasonably straight line at the half maximum point. This process is accomplished, as shown in Fig 23, by manually changing the bias on PZT #2 while observing the S/H circuit output (top trace).

Once the voltage levels are set satisfactorily, a sine wave is put into PZT #2, introducing a known path length change to the interferometer. The feedback signal is observed on the CRT of the FFT Analyzer (because of its storage capability), and plotted digitally. The feedback signal is recorded for input signals with frequencies ranging from 0.2 Hz to 70 Hz.

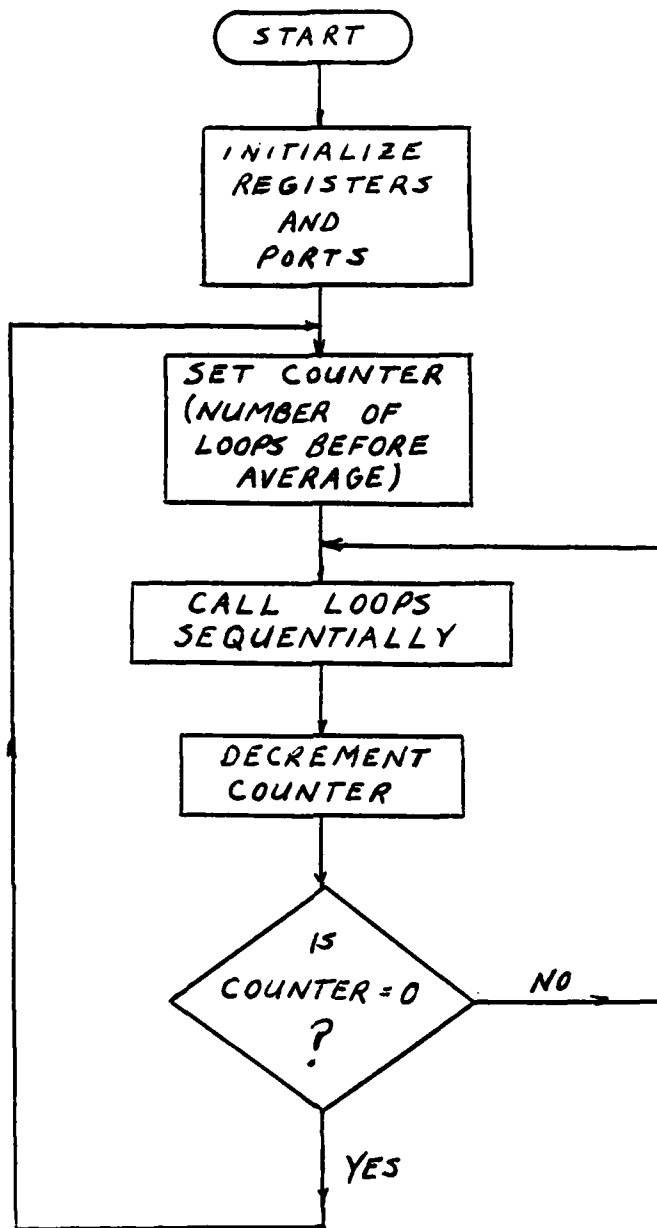


Figure 22a. Program flow diagram
(Main program)

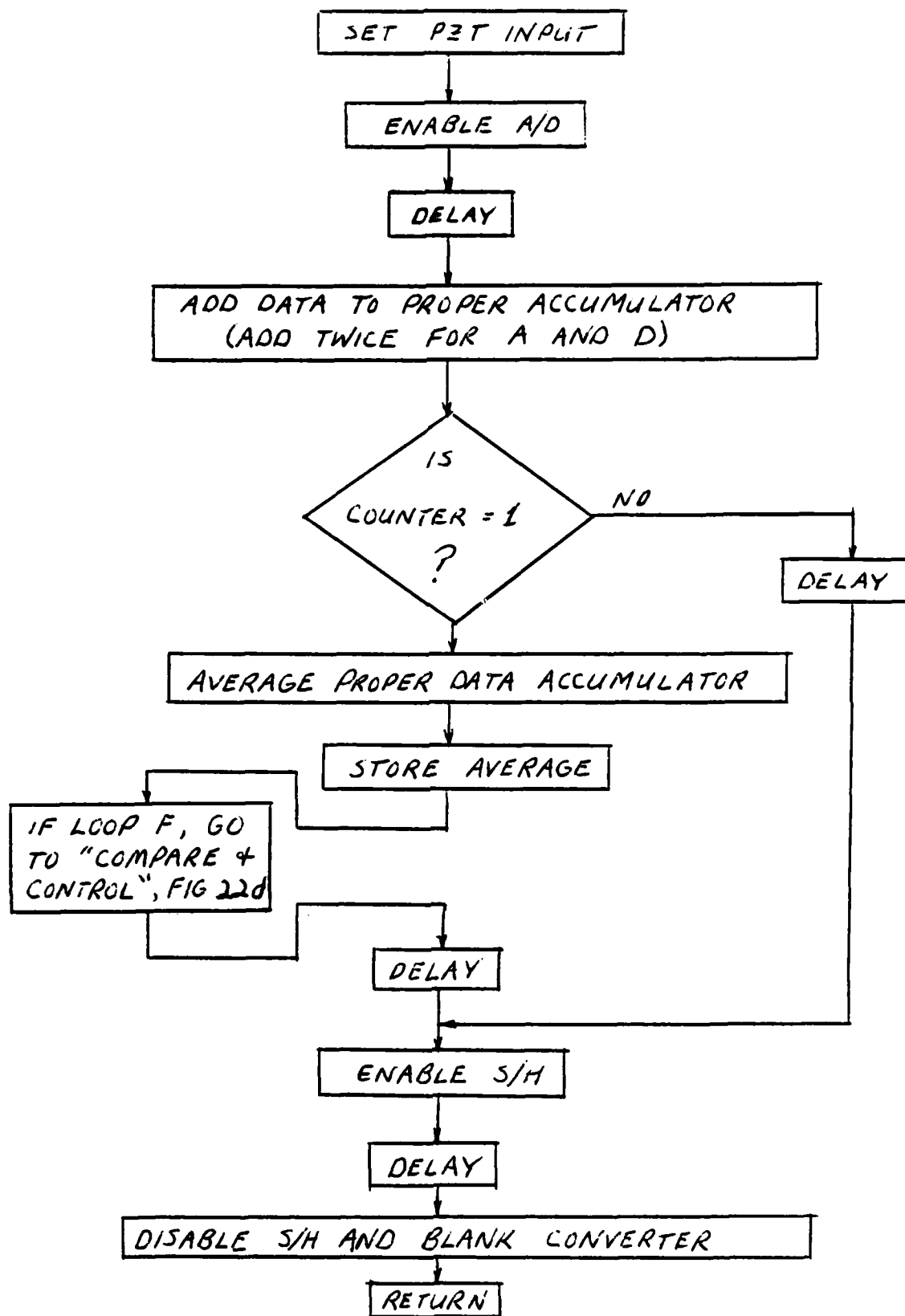


Figure 22b. Program flow diagram (Loops A,D,E and F)

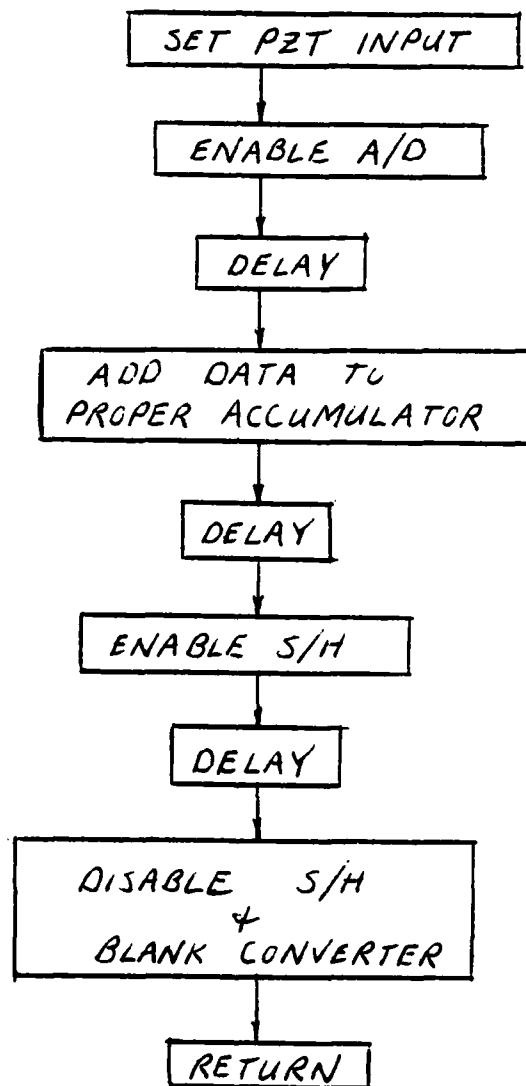


Figure 22c. Program flow diagram
(Loops B and C)

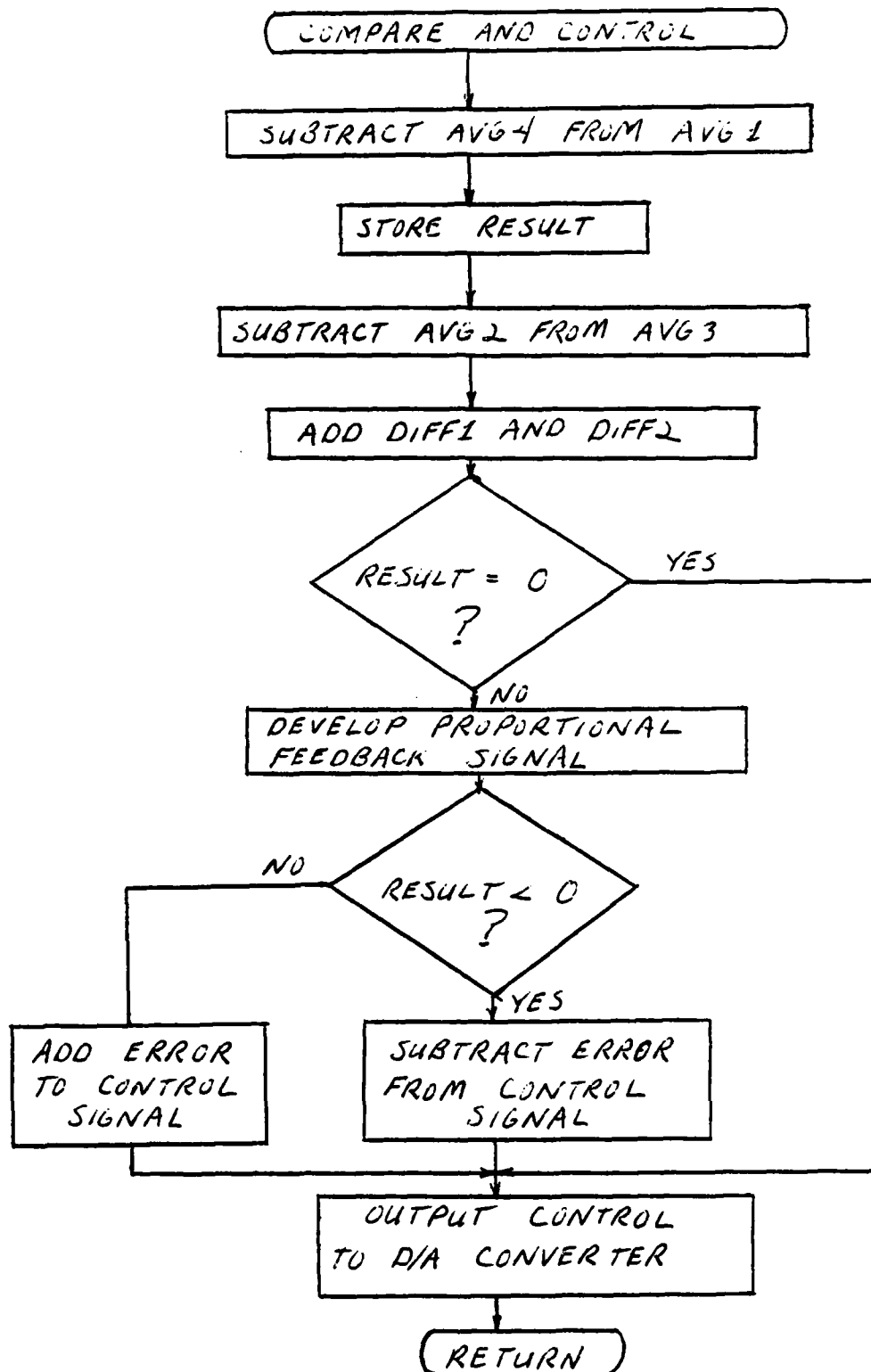


Figure 22d. Program flow diagram
(Compare and control)

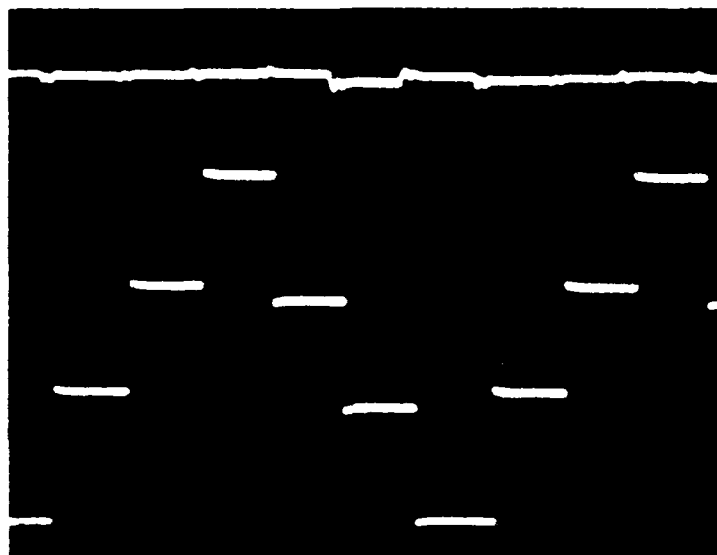


Figure 23. Sample/hold output (top trace)

V. Results

The control loop of this experiment is designed to provide a feedback signal which is proportional to a simulated rotation rate. Fig 24 shows the response of the feedback signal at different frequencies of the input signal. The input signal in each case is a 1.2 V peak to peak sine wave. At 0.2 Hz (Fig 24a), the feedback signal is following the input signal with a 180° phase shift, as expected. The feedback signal remains fairly good up to a frequency of about 10 Hz. As the frequency gets higher than 30 Hz, the digital feedback signal is not updated often enough to accurately track the simulated rotation input. This limitation can be explained in terms of Shannon's sampling theorem.

It is discovered earlier that a "safe" frequency for modulation is 500 Hz. This frequency equates to a half period of

$$\frac{T}{2} = \frac{1}{2f} = 1 \text{ msec}$$

In keeping with this limitation, the duration of each voltage level of the modified "staircase" signal is set at 1 msec. Since the test program is set up for a maximum feedback update rate of one update per program cycle (once every 6 msec), the maximum frequency that can be sampled, according to

Shannon's sampling theorem, is

$$f_{\max} = \frac{1}{2(6 \text{ msec})} = 83.33 \text{ Hz}$$

The rule of thumb for accurate representation is

$$f_{\text{thumb}} \leq \frac{1}{10(6 \text{ msec})} = 16.67 \text{ Hz}$$

It can be seen from the progression of the signals in Fig 24 that the control loop is operating well up to the sampling limit given above.

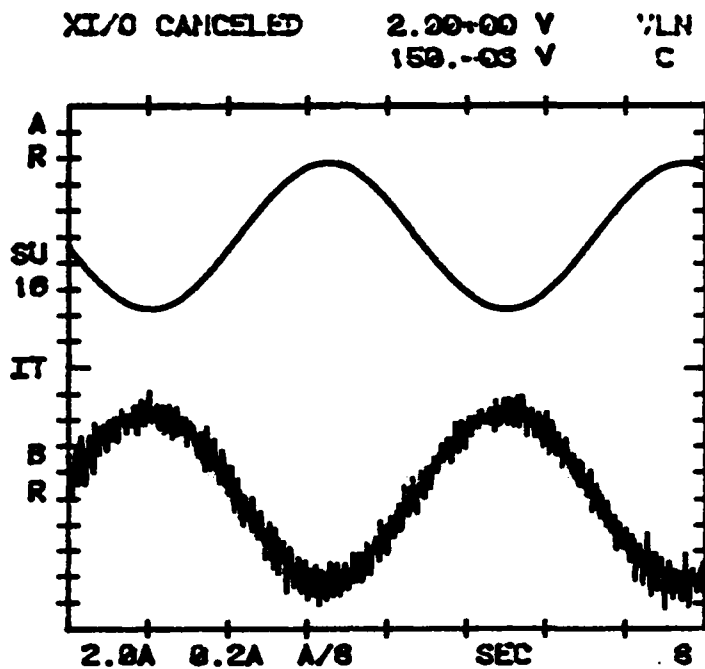


Figure 24a. Feedback signal for a simulated rotation (0.2 Hz)

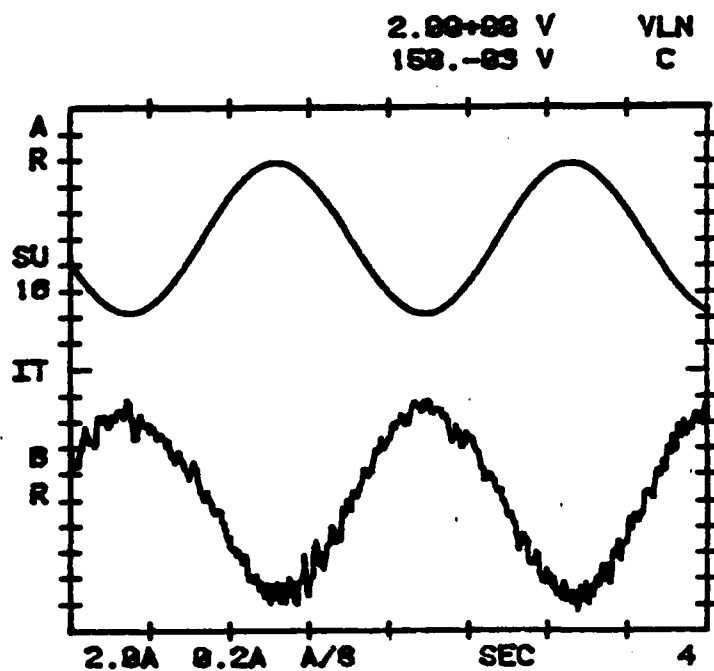


Figure 24b. Feedback signal for a simulated rotation (0.5 Hz)

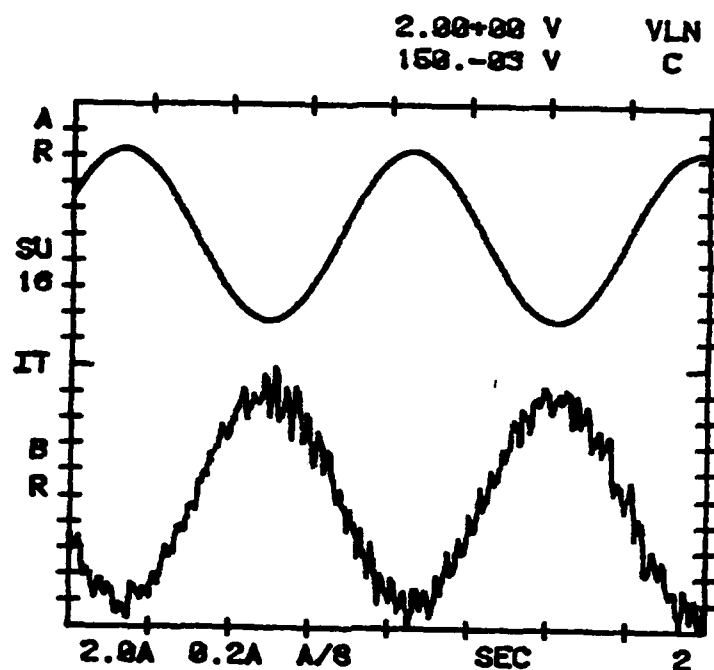


Figure 24c. Feedback signal for a simulated rotation (1 Hz)

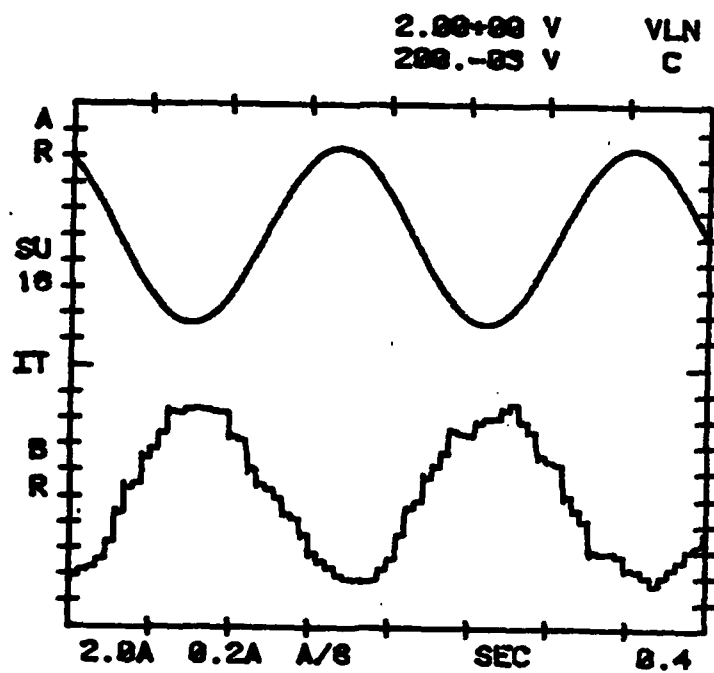


Figure 24d. Feedback signal for a simulated rotation (5 Hz)

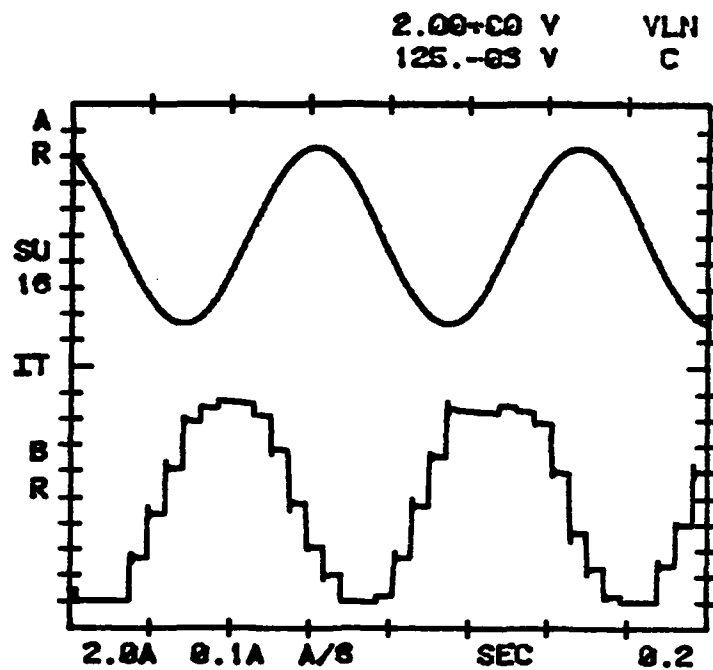


Figure 24e. Feedback signal for a simulated rotation (10 Hz)

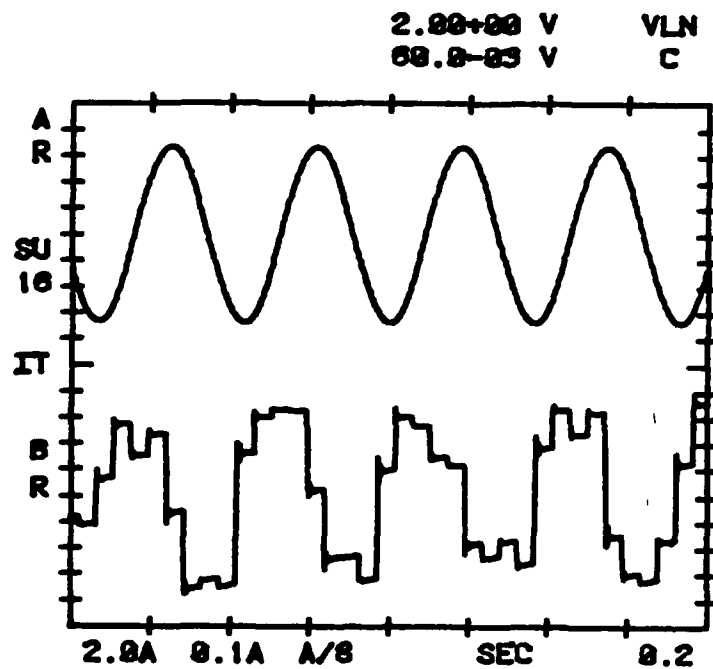


Figure 24f. Feedback signal for a simulated rotation (20 Hz)

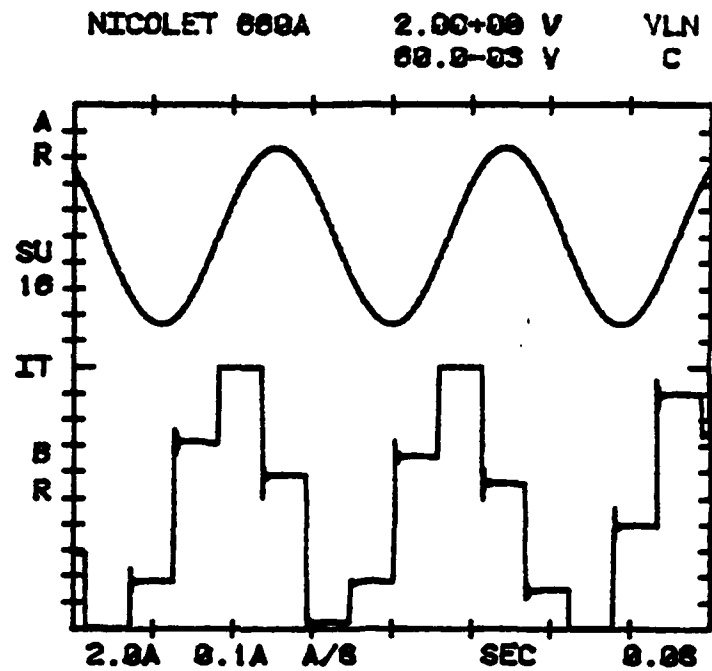


Figure 24g. Feedback signal for a simulated rotation (30 Hz)

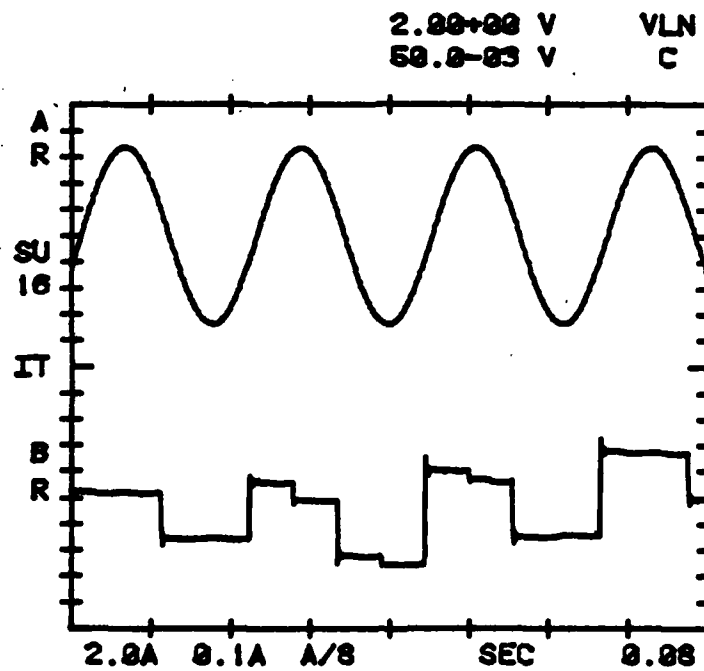


Figure 24h. Feedback signal for a simulated rotation (40 Hz)

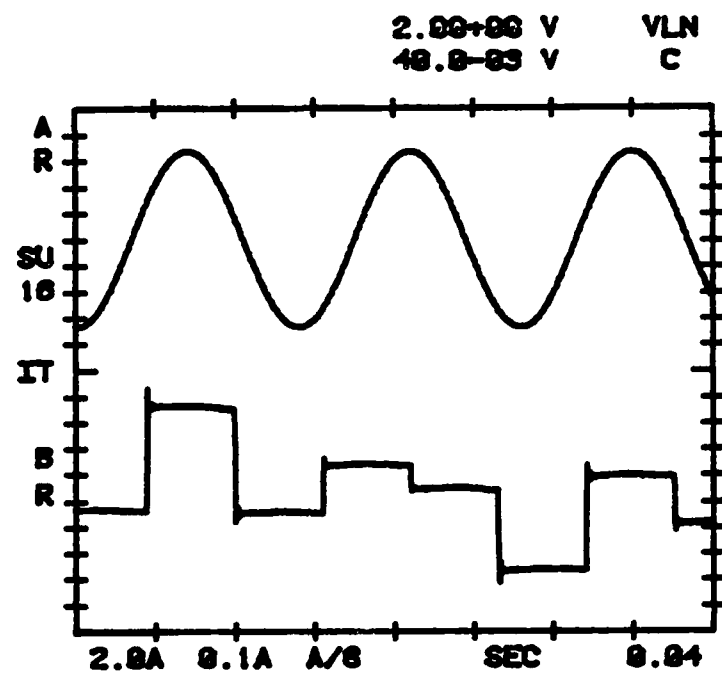


Figure 24i. Feedback signal for a
simulated rotation (70 Hz)

VI. Conclusions and Recommendations

The results bear out several conclusions, the first of which is that this method of rotation extraction is at least feasible for the fiber interferometer. The obvious recommendation immediately follows that a fiber optic Sagnac interferometer be built with the purpose of testing the amplitude modulated dither technique.

It must also be pointed out that the noise present on the 0.2 Hz feedback signal (Fig 24a) is largely due to the coarseness of the digital feedback signal. An 8-bit number just does not provide the accuracy required for the voltage levels of this experiment. This coarseness is not so much manifested in the detection circuit, but shows up more in the feedback, where 0.4 V is the smallest increment for the feedback signal. It is recommended that before the method of information extraction is implemented in a fiber optic device, a more accurate control loop be implemented in this same test setup using A/D and D/A converters of more than 8 bits.

It is also recommended that the "massage" circuit be modified to account for the 7 KHz resonant frequency appearing on the photodetector output. This improvement can be accomplished by implementing a circuit that can average the last quarter of the signal in each half cycle.

Finally, it is recommended that some experimenting be done with wavelength and intensity control using the data

available from the output intensity of the interference signal. A possible implementation might use feedback to control the wavelength of the laser light by adjusting the length of the laser cavity.

Bibliography

1. Ezekiel, S. and H. J. Arditty, editors. Fiber Optic Rotation Sensors and Related Technologies. Springer-Verlag Berlin Heidelberg New York, 1982.
2. Culshaw and Giles, "Fiber Optic Gyroscopes," Journal of Physics E: Scientific Instrumentation. Vol 16, No 1, pp 5-15, Jan 83.
3. Bohm, et al, "Low-drift fiber gyro using a superluminescent diode," Electronics Letters. Vol 17, No 10, pp 352-353, May 14, 81.
4. Pavlath, G. A. and H. J. Shaw, "Birefringence and polarization effects in fiber gyroscopes," Applied Optics. Vol 21, No 10, pp 1752-1757, May 15, 82.
5. Wickert, K. et al, "Experimental investigations of sensitivity limiting factors in an optical fiber gyro," Optics Communications. Vol 40, No 5, pp 337-341, Feb 1, 82.
6. Williamson and Wille, "Fiber Optic Gyro," AFIT Master's Thesis, Oct 79.
7. Ezekiel, S. and S. Balsamo, "Passive ring resonator laser gyroscope," Applied Physics Letters. Vol 30, No 9, p 478, May 77.
8. Arditty, H. J. and J. C. Lefevre, "Sagnac effect in fiber gyroscopes," Optics Letters. Vol 6, No 8, pp 401-403, Aug 81.
9. Bergh, R. A. et al, "All-single-mode fiber-optic gyroscope with long-term stability," Optics Letters. Vol 6, No 10, pp 502-504, Oct 81.
10. Davis, J. L. and S. Ezekiel, "Closed-loop, low noise fiber optic rotation sensor," Optics Letters. Vol 6, No 10, pp 505-507, Oct 81.
11. Bergh, R. A. et al, "All-single-mode fiber-optic gyroscope," Optics Letters. Vol 6, No 4, pp 198-200, Apr 81.
12. Bohm, K. et al, "Low-noise fiber-optic rotation sensing," Optics Letters. Vol 6, No 2, pp 64-66, Feb 81.

APPENDIX A

Sagnac Effect

The main principle behind the Sagnac interferometer was demonstrated by Sagnac himself in 1913. He postulated that rotation rate could be detected by measuring a path length difference between counter-rotating light beams traversing the same optical path. He observed the rotation rate by looking at the fringe effects due to interference between the two light beams. To illustrate this concept, consider two beams propagating in a vacuum (Fig A-1).

The counter-rotating beams (a photon in each direction) start at the same point at t_0 . While the photons are traversing the light path in opposite directions, the gyro is experiencing clockwise rotation, Ω . During the time Δt it takes for the light to pass along the path a distance L

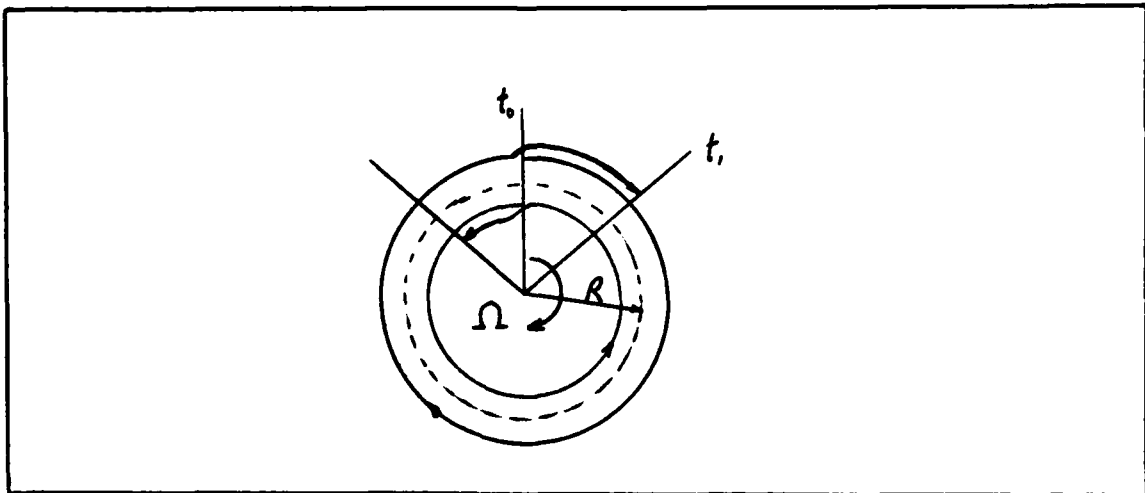


Figure A-1. Sagnac effect

(in the gyro reference frame), the photon starting point has moved a distance $\Omega R \Delta t$, where R is the radius of the circular light path. The difference in path lengths between the clockwise and counterclockwise traveling photons at time Δt is, from Fig A-1,

$$\Delta l = 2 R \Omega \Delta t \quad (\text{A-1})$$

where

$$\Delta t = \frac{2\pi R + \Delta l}{c} \quad (\text{A-2})$$

c being the speed of light in a vacuum. Substituting (A-1) into (A-2), and solving for Δl ,

$$\Delta l = \frac{4\pi R^2 \Omega}{c - R \Omega}$$

But

$$c \gg R \Omega$$

So

$$\Delta l = \frac{4\pi R^2}{c} \Omega \quad (\text{A-3})$$

and

$$\Delta t = \frac{4\pi R^2 \Omega}{c^2} \quad (\text{A-4})$$

where $A = \pi R^2$ is the area enclosed by the optical path. A fringe pattern observed at the photon starting point at time t_1 denotes a phase shift between the two light beams corresponding to

$$\Delta\phi = 2\pi \frac{\Delta t}{\lambda/c}$$

$$\Delta\phi = \frac{8\pi A}{\lambda c} \Omega \quad (\text{A-5})$$

where λ is the wavelength of the light. In the special case of fiber wound coil,

$$\Delta\phi = \frac{8\pi AN}{\lambda c} \Omega$$

where N is the number of coil windings, or

$$\Delta\phi = \frac{2\pi LD}{\lambda c} \Omega \quad (\text{A-6})$$

where $D=2R$ is the diameter of the coil. Equations (A-5) and (A-6) relate rotation rate Ω to a phase shift $\Delta\phi$. This proportionality expression, $\frac{2\pi LD}{\lambda c}$, is known as the scale factor.

APPENDIX B

Fiber Optic Sagnac Interferometer

A simple configuration of a fiber optic Sagnac interferometer (Fig B-1) divides light from a suitable light source into two equal intensity beams by means of a beamsplitter. Each beam is then coupled into one end of a fiber coil winding. The light emerging from each end of the coil is combined at the beamsplitter for detection of a difference in phase history due to rotation of the instrument.

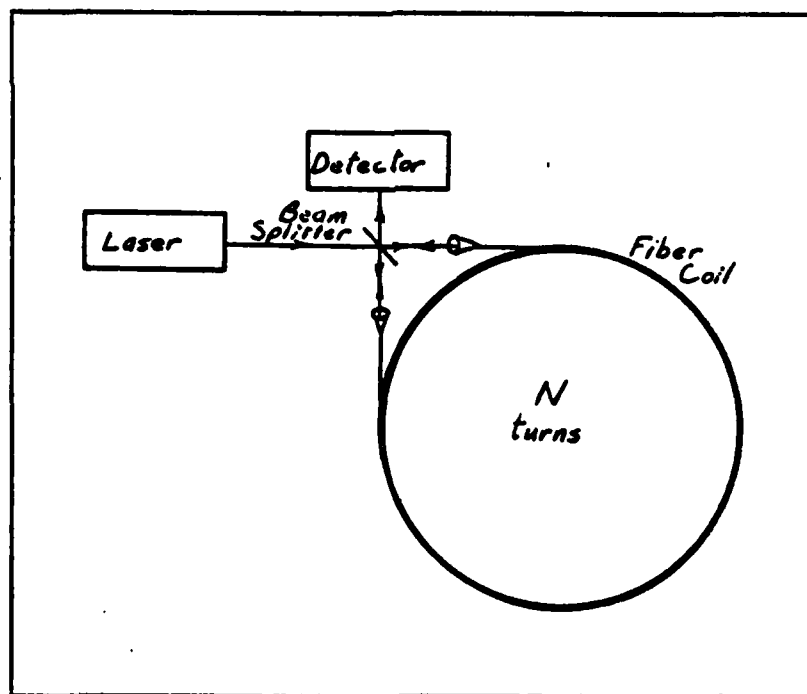


Figure B-1. Simple Sagnac interferometer

Limitations

A plot of output intensity I versus nonreciprocal phase shift $\Delta\phi$ is shown in Fig B-2 (Ref 1:8). The uncertainty in phase difference measurement $\delta(\Delta\phi)$ can be seen to be a function of the intensity noise caused by variations in the light source. Even though the operating point can be maintained where sensitivity to rotation is at a maximum (greatest change in I for small change in $\Delta\phi$), intensity noise is still appreciable. It is possible to compensate for most intensity variations in the light source except for photon shot noise, which is a random process. So, in the ideal case, the only factor limiting the instruments' sensitivity to rotation is the photon shot noise limitation (Ref 6).

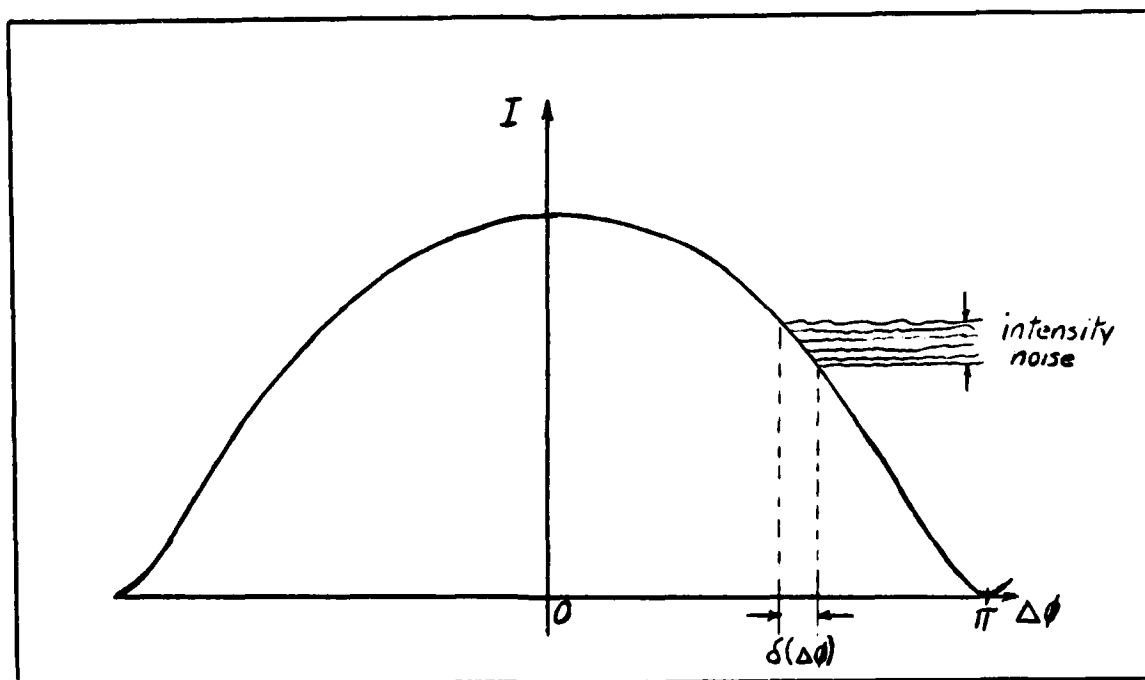


Figure B-2. Phase difference uncertainty

Reciprocity

One of the most important characteristics that a Sagnac interferometer must have for reliable operation is reciprocity. In simple terms, this means that what happens to the light traveling in one direction must happen identically to the light traveling in the opposite direction. Reciprocity is important in an optical rotation sensor because slowly varying optical path differences are being measured on the order of 10^{-15} meters over path lengths of 10^3 meters in a physical medium. This 10^{18} ratio is discouraging in light of problems like thermal expansion. Even the most thermally stable materials exhibit expansion coefficients in the 10^{-7} per degree Centigrade range, which over modest temperature ranges would generate path length changes on the order of 1 part in 10^7 - much higher than the part in 10^8 required for this measurement. What is hoped for in this device is that all parasitic effects such as the thermal expansion are reciprocal and cancel one another out since both clockwise and counterclockwise signals use the same optical path. Then the Sagnac effect, which is nonreciprocal, can be detected to small rotation rates with great reliability.

The simple Sagnac interferometer (Fig B-1) is a roughly reciprocal instrument. Because the counter-rotating light beams traverse the same optical path, reciprocal perturbations cancel out while the nonreciprocal Sagnac effect is doubled. However, experimentation with the setup proposed by Sagnac yields an interference pattern which shifts in and

out in phase with applied rotation as expected, but also drifts both in time and with temperature (Ref 1:16).

This phenomenon can be explained by a combination of the use of the beamsplitter in the interferometer and the effects of mode coupling within the fiber. Because the simple Sagnac interferometer uses a different arm for detection than it does for input, it can be shown that the phase histories of the two recombining beams differ (Ref 1:18). This is true because of the number of times each beam interacts with the beamsplitter. It turns out that the beams appearing in the detector arm interfere destructively (assuming ideal beamsplitters) for a zero rotation rate.

Another phenomenon contributing to nonreciprocity in this device is mode coupling. Whenever more than one mode is allowed to propagate through a fiber, random perturbations give rise to exchanges of energy between individual modes. This effect not only depletes the original mode of propagation energy, but also introduces to the coupled mode a phase history of light that may have travelled a different optical path.

These contributions to nonreciprocity in the simple Sagnac interferometer necessitate some changes in the original design. Fig B-3 (Ref 1:20) has incorporated the necessary changes and is the minimum reciprocal configuration.

The added beamsplitter insures that the phase histories of the two detected beams are the same. The combination of the polarizer and spatial filter restricts the entry and exit

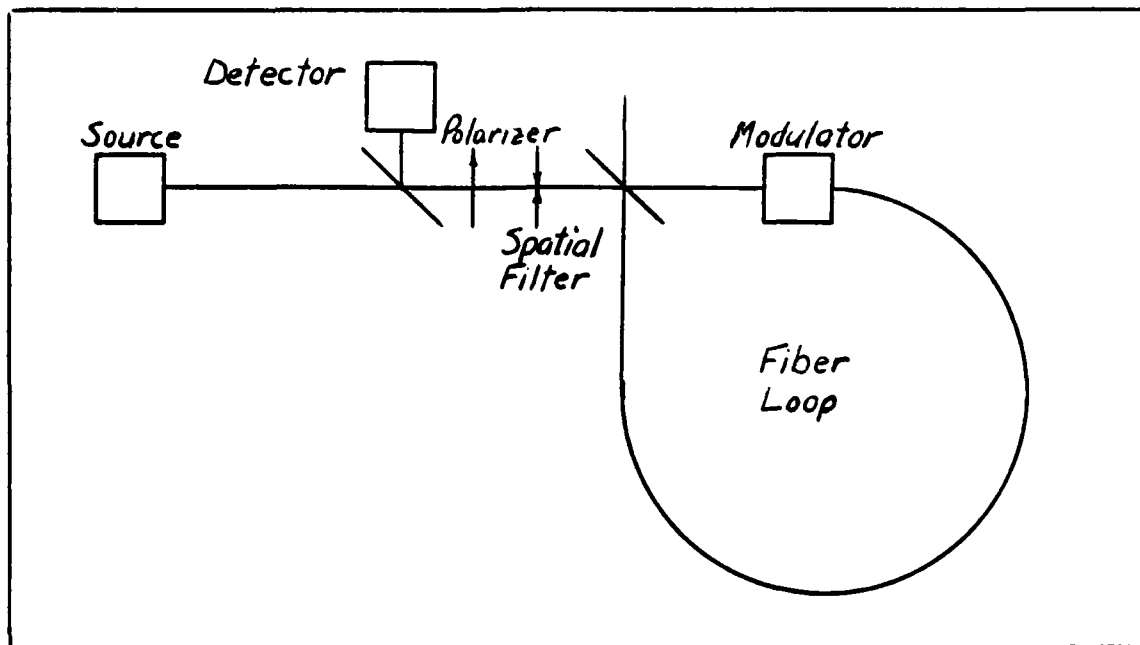


Figure B-3. Minimum reciprocal configuration.

of light into and out of the closed light path to the same mode. The modulator makes it possible, once reciprocity has been achieved, to detect and measure the Sagnac phase shift.

Error Sources

Tables B-1, B-2, and B-3 summarize the effects which cause drift, noise, and scale factor changes. They also suggest possible remedies.

Table B-1. Effects causing drift

Effect	Means to reduce effect
-Beamsplitter with free beam propagation: light beams propagating to the fiber ends and beams coming from the fiber ends do not have same axis	-Insert a good spatial filter (SM fiber filter) and use only the optical signal running back to the source -Use directional couplers, avoid freely propagating beams
-Losses in the beamsplitter or directional coupler	-Use only the optical signal running back to the source
-Birefringence of fiber (Fiber supports orthogonally polarized modes)	-Insert polarizers -Stabilization of state of polarization, use polarization preserving fibers
-Exposure of fiber to thermal radiation	-Shield fiber coil
-Magnetic field	-Shield fiber coil magnetically

Table B-2. Effects causing noise

Effect	Means to reduce effect
-Noise due to light scattering in fibers (Rayleigh) and in components	-Light source with low coherence length (multimode semiconductor diode laser), frequency modulated source
-Photodetector noise	
-1/f noise	-Phase modulation frequency greater than 1 KHz
-amplifier noise	-Low C input circuit, large R, low noise field effect transistor (FET)
-shot noise	-High power laser, low attenuation fiber, low fiber coupling losses

Table B-3. Effects causing scale factor changes

Effect	Means to reduce effect
-Fiber coil	
-Change of area A with temperature	-Sense temperature T, correct for T, stabilize T
-Change of attenuation and birefringence	-Evaluate signals such that signal amplitude has no effect on scale factor
-Laser	
-Change of laser wavelength	-Sense and correct wavelength
-Change of spectral distribution	-Use low bandwidth source
-Change of output power	-Evaluate signals such that signal amplitude has no effect on scale factor
-Effect of light returning to laser	-Insert optical isolator or attenuator, use lasers insensitive to returning light

APPENDIX C

Hardware Descriptions

Michelson Interferometer

The Michelson interferometer is built using a 2 mW Tropel HeNe laser as a light source. After a cube beam-splitter splits the beam in two directions, two totally reflecting flat Spectra-Physics mirrors reflect the light beams back to the beamsplitter where the beams interfere. The mirrors are glued to cylindrical PZTs which are mounted in adjustable mounts (two degrees of freedom). The PZT mounts and beamsplitter are bolted to a thin aluminum sheet which is in turn bolted to a 1" aluminum slab. The slab is supported on the four corners with pieces of foam rubber for isolation from vibration. A cardboard shelter is built to protect the device from wind currents which adversely affect path length data. The photodetector is a PIN-3D photodiode set up for photoconductive operation. Fig C-1 shows the bias circuit for photodetection.

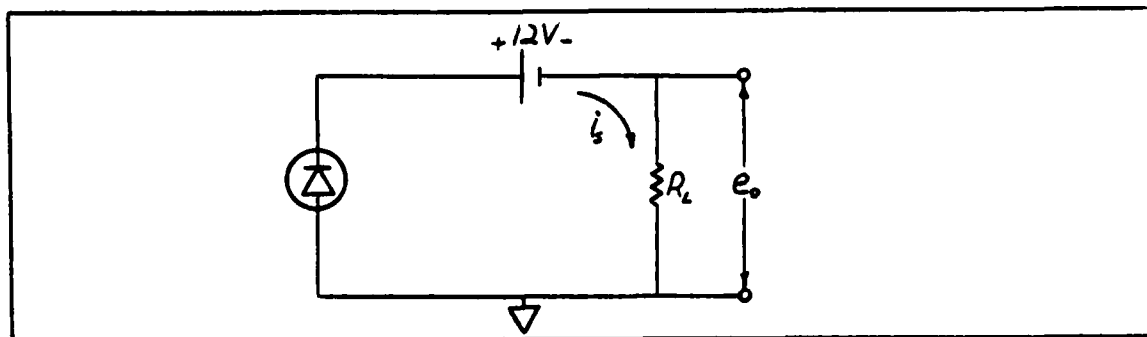


Figure C-1. Photodetector bias circuit

Feedback Control Loop

The feedback control loop is shown in Fig C-2. The signal from the photodetector is input to a 741 op-amp set up for variable gain. This amplifier acts not only as a buffer but is also used to adjust the photodetector output for a voltage range from 0-10 V.

The S/H circuit uses a 4066 bilateral switch which has very low ON resistance and high OFF resistance, making it ideal for S/H application. Since the 741 op-amp has high input resistance, the capacitor stays charged till the 4066 switch is closed. The 4066 is enabled with a software generated enable signal from I/O port 8EH, bit 2. The 7406 inverts the enable signal.

The A/D converter being used is the AD570. It is an 8-bit converter with a conversion time of 25 usec and has a 0-10 V range. The output of the A/D converter enters the computer through I/O port 8CH. The D/A converter being used is the DAC0808. It also is an 8-bit converter with a 0-10 V range and takes its input from I/O port 8AH of the computer.

Since the feedback signal out of the D/A converter eventually is amplified by a gain of 10 at the HVA, it is divided by 10 with a simple voltage divider. A 741 op-amp acts as an inverting buffer. It is necessary to have feedback on either side of zero volts, so a bias is necessary to convert the 0-1 V range to a -0.5 to +0.5 V range. This bias, along with the digitally generated modulation signal, is added to the feedback signal through a 741 op-amp set up as

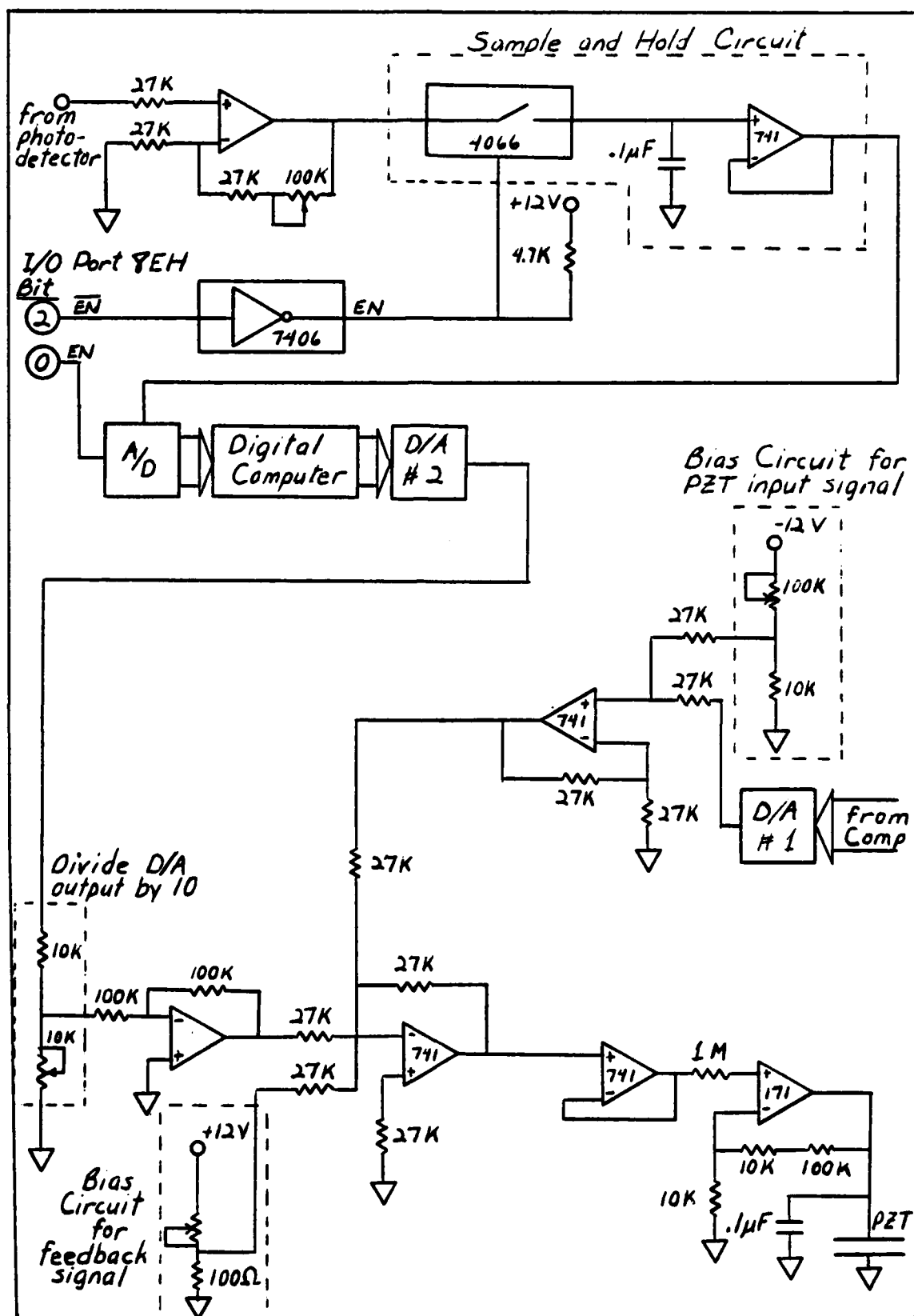


Figure C-2. Control loop schematic

an inverting summing amplifier. Another 741 is used as a buffer before the HVA stage. The HVA, set up for a gain of 10, amplifies the signal for application to the PZT. The 0.1 uF capacitor is used to help tune the PZT for suppression of its 7 KHz resonance. It should be noted that a bias circuit such as the one for the feedback signal is also built for the modulation signal for the same reason.

APPENDIX D

Feedback Control Program

This is the assembly language program which collects the rotation information, processes that information, and generates a feedback signal to maintain path length difference of the interferometer equal to zero.

Label	Instruction	Data	Comment
	MVI	A,OFFH	;MODE 3
	OUT	8DH	
	MVI	A,OFFH	;ALL IN FOR ADC PORT
	OUT	8DH	
;8CH IS NOW THE ADC	PORT		
	MVI	A,OFFH	;MODE 3
	OUT	8FH	
	MVI	A,80H	;SET LSB FOR B/C & 3rd BIT
	OUT	8FH	; FOR S/H EN
;8EH IS NOW THE ADC	CONTROL PORT		
	MVI	A,OFFH	;MODE 3
	OUT	89H	
	MVI	A,00H	;ALL OUT FOR FIRST DAC PORT
	OUT	89H	
;88H IS THE FIRST DAC	PORT		
	MVI	A,OFFH	;MODE 3
	OUT	8BH	
	MVI	A,00H	;ALL OUT FOR SECOND DAC PORT
	OUT	8BH	
;8AH IS NOW THE SECOND DAC	PORT		
;			
	MVI	A,80H	;SET "CONTROL" TO ZERO VOLTS
	STA	CONTROL	
	MVI	A,08H	
	LXI	H,DATA1	
CLR:	MVI	M,00H	;CLEAR DATA ACCUMULATORS
	INX	H	
	DCR	A	
	JNZ	CLR	
START:	MVI	C, <u>a</u>	;SET NUMBER OF CYCLES BEFORE AVERAGING

Label	Instruction	Data	Comment
BEGIN:	MVI	A,62H	
	CALL	LOOPA	
	MVI	A,A8H	
	CALL	LOOPB	
	MVI	A,F2H	;SET VALUES FOR
	CALL	LOOPC	; PZT INPUT LEVELS
	MVI	A,9EH	
	CALL	LOOPD	
	MVI	A,57H	
	CALL	LOOPE	
	MVI	A,0EH	
	CALL	LOOPF	
	DCR	C	
	JNZ	BEGIN	;CONTINUE LOOPING
	JMP	START	;START NEW AVERAGING CYCLE
LOOPA:	OUT	88H	;SET PZT INPUT
	MVI	A,FEH	;ENABLE A/D
	OUT	8EH	
	MVI	B,14H	
LP1:	DCR	B	
	JNZ	LP1	;ALLOW A/D CONVERSION TIME
	IN	8CH	;GET DATA FROM A/D
	MOV	E,A	
	MVI	D,00H	;KEEP RUNNING SUM IN DATA1
	LHLD	DATA1	
	DAD	DE	
	DAD	DE	
	SHLD	DATA1	
	MOV	A,C	;READY TO AVERAGE YET?
	CPI	01H	
	JZ	AVER1	
LP2:	MVI	B,0A9H	
	DCR	B	;IF NOT ENOUGH SAMPLES,
	JNZ	LP2	; DELAY FOR TIMING
	JMP	SKIP1	
AVER1:	LHLD	DATA1	
	CALL	AVG	;AVERAGE DATA1
	STA	AVG1	
	MVI	B,97H	;DELAY FOR TIMING
LP3:	DCR	B	
	JNZ	LP3	
SKIP1:	MVI	A,FAH	;ENABLE S/H
	OUT	8EH	
	MVI	B,3EH	

Label	Instruction	Data	Comment
LP4:	DCR JNZ	B LP\$;ALLOW TIME FOR S/H
	MVI OUT	A,FFH 8EH	;DISABLE S/H & BLANK CONVERTER
	RET		
LOOPB:	OUT MVI OUT MVI	88H A,FEH 8EH B,14H	;SET PZT INPUT ;ENABLE A/D
LP5:	DCR JNZ	B LP5	;ALLOW A/D CONVERSION
	IN	8CH	;GET DATA FROM A/D
	MOV MVI LHLD DAD SHLD	E,A D,00H DATA2 DE DATA2	;KEEP RUNNING SUM IN DATA2
LP6:	MVI DCR JNZ	B,0ACH B LP6	;DELAY
	MVI OUT	A,FAH 8EH	;ENABLE S/H
LP7:	MVI DCR JNZ	B,3EH B LP7	;ALLOW TIME FOR S/H
	MVI OUT	A,FFH 8EH	;DISABLE S/H & BLANK CONVERTER
	RET		
LOOPC:	OUT MVI OUT MVI	88H A,FEH 8EH B,14H	;SET PZT INPUT ;ENABLE A/D
LP8:	DCR JNZ	B LP8	;ALLOW A/D CONVERSION TIME
	IN	8CH	;GET DATA FROM A/D
	MOV MVI	E,A D,00H	

Label	Instruction	Data	Comment
	LHLD	DATA3	;KEEP RUNNING SUM IN DATA3
	DAD	DE	
	SHLD	DATA3	
LP9:	MVI	B,0ACH	
	DCR	B	;DELAY
	JNZ	LP9	
	MVI	A,FAH	:ENABLE S/H
	OUT	8EH	
LP10:	MVI	B,3EH	
	DCR	B	;ALLOW TIME FOR S/H
	JNZ	LP10	
	MVI	A,FFH	;DISABLE S/H & BLANK CONVERTER
	OUT	8EH	
	RET		
LOOPD:	OUT	88H	;SET PZT INPUT
	MVI	A,FEH	;ENABLE A/D
	OUT	8EH	
LP11:	MVI	B,14H	
	DCR	B	;ALLOW A/D CONVERSION TIME
	JNZ	LP11	
	IN	8CH	;GET DATA FROM A/D
	MOV	E,A	
	MVI	D,00H	
	LHLD	DATA4	;KEEP RUNNING SUM IN DATA4
	DAD	DE	
	DAD	DE	
	SHLD	DATA4	
	MOV	A,C	;IS IT TIME TO AVERAGE?
	CPI	01H	
	JZ	AVER4	
LP12:	MVI	B,0A9H	
	DCR	B	;DELAY FOR TIMING
	JNZ	LP12	
	JMP	SKIP2	
AVER4:	LHLD	DATA4	
	CALL	AVG	;AVERAGE DATA4
	STA	AVG4	
LP13:	MVI	B,97H	
	DCR	B	;DELAY
	JNZ	LP13	

Label	Instruction	Data	Comment
SKIP2:	MVI OUT	A,FAH 8EH	;ENABLE S/H
LP14:	MVI DCR JNZ	B,3EH B LP14	;ALLOW TIME FOR S/H
	MVI OUT	A,FFH 8EH	;DISABLE S/H & BLANK CONVERTER
	RET		
LOOPE:	OUT MVI OUT	88H A,FEH 8EH	;SET PZT INPUT ;ENABLE A/D
LP15:	MVI DCR JNZ	B,14H B LP15	;ALLOW A/D CONVERSION TIME
	IN	8CH	;GET DATA
	MOV MVI LHLD DAD SHLD	E,A D,00H DATA3 DE DATA3	;KEEP RUNNING SUM IN DATA3
	MOV CPI JZ	A,C 01H AVER3	;READY TO AVG?
LP16:	MVI DCR JNZ JMP	B,0AAH B LP16 SKIP3	;DELAY
AVER3:	LHLD CALL STA	DATA3 AVG AVG3	;AVERAGE DATA3
LP17:	MVI DCR JNZ	B,98H B LP17	;DELAY
SKIP3:	MVI OUT	A,FAH 8EH	;ENABLE S/H
LP18:	MVI DCR JNZ	B,3EH B LP18	;DELAY

Label	Instruction	Data	Comment
	MVI	A, FFFH	;DISABLE S/H & BLANK CONVERTER
	OUT	8EH	
	RET		
LOOPF:	OUT	88H	;SET PZT INPUT
	MVI	A, FEH	;ENABLE A/D
	OUT	8EH	
LP19:	MVI	B, 14H	
	DCR	B	;DELAY
	JNZ	LP19	
	IN	8CH	;GET DATA
	MOV	E, A	
	MVI	D, 00H	
	LHLD	DATA2	;KEEP RUNNING SUM IN DATA2
	DAD	DE	
	SHLD	DATA2	
	MOV	A, C	
	CPI	01H	;READY TO AVG?
	JZ	AVER2	
LP20:	MVI	B, 0ACH	
	DCR	B	;DELAY
	JNZ	LP20	
	JMP	SKIP4	
AVER2:	LHLD	DATA2	
	CALL	AVG	;AVERAGE DATA2
	STA	AVG2	
LP21:	MVI	B, 76H	
	DCR	B	;DELAY
	JNZ	LP21	
CONTROL:	LDA	AVG1	;ADD AVG1 AND AVG3
	MOV	E, A	; AND STORE IN DATA1
	MVI	D, 00H	
	LDA	AVG3	
	MOV	L, A	
	MVI	H, 00H	
	DAD	DE	
	SHLD	DATA1	
	LDA	AVG2	
	MOV	E, A	
	MVI	D, 00H	;ADD AVG2 . AVG4
	LDA	AVG4	
	MOV	L, A	

Label	Instruction	Data	Comment
	MVI	H,00H	
	DAD	DE	
	MOV	A,H	
	CMA		;GET 2"s COMPLEMENT OF
	MOV	H,A	; AVG2 + AVG4
	MOV	A,L	
	CMA		
	MOV	L,A	
	INX	H	
	MOV	D,H	
	MOV	E,L	;PERFORM ADDITION
	LHLD	DATA1	
	DAD	DE	
	JC	CONT1	;IS RESULT NEG OR POS
	MOV	A,H	;IF RESULT LT ZERO, 2"s COMPL
	CMA		
	MOV	H,A	
	MOV	A,L	
	CMA		
	MOV	L,A	
	INX	HL	
	MVI	A,01H	;SET SIGN TO "1" FOR NEG
	STA	SIGN	
	JMP	CONT2	
CONT1:	MVI	A,00H	;SET SIGN TO "0" FOR POS
	STA	SIGN	
CONT3:	MVI	B,02H	
	DCR	B	;DELAY
	JNZ	CONT3	
CONT2:	MOV	A,H	
	CPI	01H	
	CMC		
	MOV	A,L	
	MVI	B,1 or 2	;DIVIDE BY 2 or 4
CONT4:	RAR		
	STC		
	CMC		
	DCR	B	
	JNZ	CONT4	
	MOV	B,A	;STORE ERROR SIGNAL
	CPI	0H	
	JZ	LT	;IF WITHIN LSB, DON'T UPDATE
	LDA	SIGN	
	CPI	01H	
	JZ	NEG	

Label	Instruction	Data	Comment
POS:	LDA	CONTROL	;POS ERROR?
	ADD	B	;INCREASE CONTROL
	JMP	CONT5	;
NEG:	LDA	CONTROL	;NEG ERROR?
	SUB	B	;DECREASE CONTROL
CONT5:	OUT	8AH	
	STA	CONTROL	
	JMP	CONT6	
LT:	MVI	B,05H	
LT1:	DCR	B	;DELAY
	JNZ	LT1	
CONT6:	MVI	A,08H	
	LXI	H,DATA1	
CLR:	MVI	M,00H	;CLEAR DATA
	INX	H	
	DCR	A	
	JNZ	CLR	
SKIP4:	MVI	A,FAH	;ENABLE S/H
	OUT	8EH	
LP22:	MVI	B,3EH	
	DCR	B	;DELAY
	JNZ	LP22	
	MVI	A,FFH	;DISABLE S/H & BLANK CONVERTER
	OUT	8EH	
	RET		
AVG:	STC		
	CMC		
	MOV	A,L	
	MVI	B, <u>b</u>	
DVD:	RAR		
	STC		
	CMC		
	DCR	B	
	JNZ	DVD	
	MOV	D,A	
	MOV	A,H	
	STC		
	CMC		
	MVI	B, <u>c</u>	
DVD1:	RAL		
	STC		
	CMC		

Label	Instruction	Data	Comment
	DCR	B	
	JNZ	DVD1	
	ADD	D	
	RET		
DATA1:	.WORD		
DATA2:	.WORD		
DATA3:	.WORD		
DATA4:	.WORD		
AVG1:	.BYTE		
AVG2:	.BYTE		
AVG3:	.BYTE		
AVG4:	.BYTE		
CONTROL:	.BYTE		
SIGN:	.BYTE		

Values that need to be set

a	b	c
1	1	7
2	2	6
4	3	5
8	4	4
10H	5	3
20H	6	2
40H	7	1

a represents the number of cycles before averaging.

VITA

Daniel John Brett was born on 22 May 1955 in Los Angeles, California. He graduated from high school in Durango, Colorado in 1973 and enlisted in the Air Force on October 1973. After completing basic training and technical school, he was stationed at Ellsworth AFB, South Dakota, where he served as an automatic flight control systems specialist in the 28th Avionics Maintenance Squadron. Leaving the Air Force in October 1977, he attended South Dakota School of Mines and Technology, from which he received a Bachelor of Science in Electrical Engineering in December 1981. He reentered the Air Force on active duty in January 1982 and received his commission from Officer Training School in April 1982. He entered the School of Engineering, Air Force Institute of Technology, in June 1982.

Permanent address: 590 County Road 207
Durango, Colorado 81301

UNCLASSIFIED

SECURITY CLASSIFICATION OF THIS PAGE

REPORT DOCUMENTATION PAGE

1. REPORT SECURITY CLASSIFICATION Unclassified			1b. RESTRICTIVE MARKINGS	
2a. SECURITY CLASSIFICATION AUTHORITY			3. DISTRIBUTION/AVAILABILITY OF REPORT Approved for public release; distribution unlimited.	
2b. DECLASSIFICATION/DOWNGRADING SCHEDULE				
4. PERFORMING ORGANIZATION REPORT NUMBER(S) AFIT/GE/EE/83D-12			5. MONITORING ORGANIZATION REPORT NUMBER(S)	
6a. NAME OF PERFORMING ORGANIZATION School of Engineering		6b. OFFICE SYMBOL (If applicable) AFIT/EN	7a. NAME OF MONITORING ORGANIZATION	
6c. ADDRESS (City, State and ZIP Code) Air Force Institute of Technology Wright-Patterson AFB, Ohio 45433			7b. ADDRESS (City, State and ZIP Code)	
8a. NAME OF FUNDING/SPONSORING ORGANIZATION		8b. OFFICE SYMBOL (If applicable)	9. PROCUREMENT INSTRUMENT IDENTIFICATION NUMBER	
8c. ADDRESS (City, State and ZIP Code)			10. SOURCE OF FUNDING NOS.	
11. TITLE (Include Security Classification) See Box 19			PROGRAM ELEMENT NO.	
			PROJECT NO.	
			TASK NO.	
			WORK UNIT NO.	
12. PERSONAL AUTHOR(S) Daniel J. Brett, B.S., 2Lt, USAF				
13a. TYPE OF REPORT MS Thesis		13b. TIME COVERED FROM _____ TO _____	14. DATE OF REPORT (Yr., Mo., Day) 1983 December	15. PAGE COUNT 82
16. SUPPLEMENTARY NOTATION				
Approved for public release: IAW AFR 190-17. LYNN E. WOLNER 7 Feb 84 Dept. for Research and Professional Development Wright-Patterson AFB OH 45433				
17. COSATI CODES			18. SUBJECT TERMS (Continue on reverse if necessary and identify by block number)	
FIELD	GROUP	SUB. GR.		
17	08		LASER GUIDANCE, GYROSCOPES, FIBER OPTICS	
19. ABSTRACT (Continue on reverse if necessary and identify by block number)				
Title: Extraction of Rotation Information from a Simulated Fiber Optic Gyro Using Amplitude Modulation Thesis Chairman: Salvatore Balsamo, Major, USAF				
20. DISTRIBUTION/AVAILABILITY OF ABSTRACT UNCLASSIFIED/UNLIMITED <input checked="" type="checkbox"/> SAME AS RPT. <input type="checkbox"/> DTIC USERS <input type="checkbox"/>			21. ABSTRACT SECURITY CLASSIFICATION UNCLASSIFIED	
22a. NAME OF RESPONSIBLE INDIVIDUAL Salvatore Balsamo, Major, USAF			22b. TELEPHONE NUMBER (Include Area Code) AV 259-3122	22c. OFFICE SYMBOL FJSRL/NH

UNCLASSIFIED

SECURITY CLASSIFICATION OF THIS PAGE

The purpose of this experiment was to determine feasibility of the amplitude modulated dither technique of extracting rotation information from a fiber optic gyroscope. By varying the amplitude of the modulation appropriately, information can be obtained at points on the output intensity curve that are most sensitive to rotation. These points are also in the most linear region of the curve.

A Michelson interferometer is used to simulate a Sagnac interferometer undergoing rotation. A digital control loop processes the information obtained by amplitude modulation and generates a feedback signal to null the path length difference.

The feedback signal is monitored while a rotation simulation signal is introduced to the interferometer. The feedback signal tracks the simulation signal at 180 out of phase (negative feedback). The test setup performs as expected to the hardware and operating frequency limits.

SECURITY CLASSIFICATION OF THIS PAGE

END

FILMED

384

DTIC